

Aus der Klinik für Neurologie  
Lehr- und Forschungsgebiet Physik der Magnetresonanztomographie in den  
Neurowissenschaften  
Leiter Univ.-Prof. Nadim Joni Shah, PhD

Combined EEG and fMRI for the investigation of loudness dependence of  
auditory evoked potentials (LDAEP)

Von der Medizinischen Fakultät  
der Rheinisch-Westfälischen Technischen Hochschule Aachen  
zur Erlangung des akademischen Grades eines Doktors der Medizin genehmigte  
Dissertation

vorgelegt von

Jorge Andrés Arrubla Martínez  
aus Medellín (Kolumbien)

Berichter: Univ.-Prof. Nadim Joni Shah, PhD  
Univ.-Prof. Dr. med. Hans Clusmann

Tag der mündlichen Prüfung: 11.08.2015

***Diese Dissertation ist auf den Internetseiten der Hochschulbibliothek online  
verfügbar.***



Rheinisch-Westfaelische Technische Hochschule  
Medizinische Fakultät

Thesis to achieve the academic degree Dr. med

**Combined EEG and fMRI for the investigation of  
loudness dependence of auditory evoked potentials  
(LDAEP)**

Student:	Jorge Andrés Arrubla Martínez
Birth date:	04.06.1986
Place of birth:	Medellín, Colombia
E-Mail:	jorgearrubla@yahoo.com

Supervisor: Univ.-Prof. Nadim Joni Shah, PhD





Disclosure: part of this study was included in the publication entitled “Cortical response variation with different sound pressure levels: a combined event-related potentials and FMRI study”, by Neuner et al. (PLoS One, 9(10): e109216, 2014).

# Table of Contents

1 Introduction.....	1
1.1 Electrophysiology, functional imaging and multimodal techniques .....	1
1.2 Auditory evoked potentials and their clinical significance.....	5
1.3 Integrating the ERP information into the LDAEP fMRI data analysis.....	8
1.4 Hypotheses.....	9
2 Methods.....	11
2.1 Subjects and measurements.....	11
2.2 EEG data analysis.....	13
2.2.1 Determination of the LDAEP.....	14
2.3 fMRI data analysis.....	14
2.3.1 Single-level analysis.....	15
2.3.2 Higher-level analysis.....	15
2.3.3 Repeated measures ANOVA.....	16
2.3.4 Region of Interest analysis.....	17
3 Results.....	18
3.1 EEG data analysis.....	18
3.1.1 Auditory evoked potentials.....	18
3.1.2 LDAEP calculation.....	18
3.2 Functional data analysis.....	18
3.2.1 Higher-level analysis of the functional data.....	18
3.2.2 Inclusion of the AEPs amplitudes into the fMRI analysis...	20

3.2.3 ROI analysis.....	21
3.2.4 Repeated measures ANOVA.....	21
3.2.5 Comparison of High and Low intensity tones.....	22
4 Discussion.....	23
4.1 Effectiveness of the auditory stimulation.....	23
4.2 Correlation between the AEP amplitudes and the extent of fMRI cortical response.....	23
4.3 Involvement of cortical structures in sounds perception and LDAEP.....	24
4.4 Limitations of the study.....	27
5 Conclusion.....	28
6 Acknowledgments.....	29
7 Figures.....	30
8 Tables.....	45
9 Bibliography.....	58
10 Appendices.....	I

## List of Figures

Fig. 1: MR compatible EEG cap.....	30
Fig. 2: Methodological approach for fMRI data analysis.....	31
Fig. 3: Masks of the regions of interest (ROI) created according to the Harvard-Oxford cortical structural atlas.....	32
Fig. 4: Grand average ( $n = 16$ ) of the auditory evoked related potentials for the different sound pressure levels at Cz measured inside the scanner.....	33
Fig. 5: Mixed effects group analysis ( $n = 16$ ) of the fMRI activation related to the 70 dB stimuli.....	34
Fig. 6: Mixed effects group analysis ( $n = 16$ ) of the fMRI activation related to the 80 dB stimuli.....	35
Fig. 7: Mixed effects group analysis ( $n = 16$ ) of the fMRI activation related to the 90 dB stimuli.....	36
Fig. 8: Mixed effects group analysis ( $n = 16$ ) of the fMRI activation related to the 100 dB stimuli.....	37
Fig. 9: Voxel-wise statistical map of the significant clusters showing covariance with N1/P2 amplitudes at 70 dB.....	38
Fig. 10: Voxel-wise statistical map of the significant clusters showing covariance with N1/P2 amplitudes at 80 dB.....	39
Fig. 11: Voxel-wise statistical map of the significant clusters showing covariance with N1/P2 amplitudes at 90 dB.....	40

Fig. 12: Voxel-wise statistical map of the significant clusters showing covariance with N1/P2 amplitudes at 100 dB.....	41
Fig. 13: Number of activated voxels within the ROI at each sound pressure for fMRI alone analysis and EEG-informed fMRI analysis..	42
Fig. 14: Repeated measures ANOVA of 1 factor at 4 levels.....	43
Fig. 15: Fixed effects statistical map of EEG-informed group analysis (n = 16) showing additional clusters in high vs. low intensity tones. Statistically significant voxels were thresholded at $p < 0.05$ .....	44

# List of Tables

Tab. 1: Descriptive statistics of N1 and P2 ERPs.....	45
Tab. 2: Clusters of maximum with the 70 dB tones in the fMRI data analysis. Structures defined according to the Harvard-Oxford Cortical and Subcortical Structural Atlases.....	46
Tab. 3: Clusters of maximum with the 80 dB tones in the fMRI data analysis. Structures defined according to the Harvard-Oxford Cortical and Subcortical Structural Atlases.....	47
Tab. 4: Clusters of maximum with the 90 dB tones in the fMRI data analysis. Structures defined according to the Harvard-Oxford Cortical and Subcortical Structural Atlases.....	48
Tab. 5: Clusters of maximum with the 100 dB tones in the fMRI data analysis. Structures defined according to the Harvard-Oxford Cortical and Subcortical Structural Atlases.....	49
Tab. 6: Clusters with maximal covariance with N1/P2 amplitudes at 70 dB in the fMRI data analysis. Structures defined according to the Harvard-Oxford Cortical and Subcortical Structural Atlases.....	50
Tab. 7: Clusters with maximal covariance with N1/P2 amplitudes at 80 dB in the fMRI data analysis. Structures defined according to the Harvard-Oxford Cortical and Subcortical Structural Atlases.....	51
Tab. 8: Clusters with maximal covariance with N1/P2 amplitudes at 90 dB in the fMRI data analysis. Structures defined according to the Harvard-Oxford Cortical and Subcortical Structural Atlases.....	52

Tab. 9: Clusters with maximal covariance with N1/P2 amplitudes at 100 dB in the fMRI data analysis. Structures defined according to the Harvard-Oxford Cortical and Subcortical Structural Atlases.....	53
Tab. 10: Complete list of the structures which exhibited activation with the four sound pressure levels in both analyses.....	54
Tab. 11: Number of activated voxels ( $Z > 2.3$ ) in the selected ROIs.	55
Tab. 12: Cluster exhibiting significant intensity variation in the ANOVA . Structures defined according to the Harvard-Oxford Cortical and Subcortical Structural Atlases.....	56
Tab. 13: Clusters exhibiting significant statistical difference in High > Low. Structures defined according to the Harvard-Oxford Cortical and Subcortical Structural Atlases.....	57

## Appendices

Appendix I: Motion parameters of the single-level analyses.....I



## List of Abbreviations and Symbols

AAS	Average artefact subtraction
ACC	Anterior cingulate cortex
AEP	Auditory evoked potential
ANOVA	Analysis of variance
dB	Decibel
DSA	Dipole source analysis
EEG	Electroencephalography
ERP	Evoked related potential
fMRI	Functional magnetic resonance imaging
GLM	General linear model
ICA	Independent component analysis
LDAEP	Loudness dependence of auditory evoked potentials
MFC	Middle frontal cortex
OBS	Optimal basis set
OFC	Orbito-frontal cortex
PAC	Primary auditory cortex
PVC	Primary visual cortex
ROI	Region-of-interest
RPER	Rapid-presentation event-related
SSRI	Selective serotonin reuptake inhibitors
V	Volt
$\Omega$	Ohm

## Abstract

**Introduction:** Simultaneous recording of electroencephalography (EEG) and functional magnetic resonance imaging (fMRI) provides high spatial and temporal resolution. In this study EEG and fMRI were combined to investigate the structures involved in the processing of rising sound pressure levels.

**Methods:** EEG data were recorded simultaneously with fMRI from 16 healthy volunteers using MR compatible devices at 3 T. Tones with different pressure levels were delivered to the volunteers and the evoked N1/P2 amplitudes were included as covariates into the fMRI data analysis in order to compare the brain responses with high and low intensity tones. Additionally, analysis of variance (ANOVA) and region-of-interest (ROI) analysis were performed.

**Results:** The integration of the ERP parameters into the fMRI analysis showed an extended map of areas with covariance of the N1/P2 amplitudes and the BOLD signal related to the auditory stimuli. The ANOVA and ROI analyses also revealed additional brain areas apart from the primary auditory cortex (PAC) which were active with the auditory stimulation.

**Discussion:** The PAC and the insula play an important role in the processing of rising sound pressure levels. Additional activations of the anterior cingulate cortex, the opercular cortices and the orbito-frontal cortex were induced by the high intensity tones. A

strong response of the visual cortex was also found with the high intensity tones, suggesting the presence of cross-modal effects.

*Fata viam inveniunt...*

# **1 Introduction**

## **1.1 Electrophysiology, functional imaging and multimodal techniques**

Simultaneous recording of electroencephalography (EEG) and functional magnetic resonance imaging (fMRI) has shown a number of advantages that make this multimodal technique superior to fMRI alone (Makeig et al., 2004; Debener et al., 2006; Debener and Hermann 2008; Blinowska et al., 2009; Ostwald et al., 2010; Debener and de Vos 2011; Logothetis, 2012). The possibility of integrating the single trial information provided by the EEG into the fMRI analyses can enrich the results and add new perspectives to the investigation of brain function. Recording these multiple measures of brain activity at the same time, under the same physiological and psychological conditions is advantageous for many aspects of cognitive neuroscience, in particular, pharmacological challenge studies, sleep studies, studies investigating epilepsy or evoked potential studies such as P300 with regard to age (Debener and Hermann, 2008; Koike et al., 2011; Juckel et al., 2012).

Functional MRI is based on the blood oxygenation level-dependent (BOLD) contrast (Ogawa et al., 1990). The model of the haemodynamic response posits that there are three phases of the BOLD response to a transient increase in neuronal activity: an initial, small decrease in image intensity below baseline (during the initial period of oxygen consumption), followed by a large increase above baseline (an oversupply of oxygenated blood, which is only

partially compensated for by an increase in deoxygenated venous blood volume), and then by a decrease below baseline before returning to baseline again (Heeger and Rees, 2002). Thus, fMRI is a technique with high spatial-resolution, but lacks of good temporal-resolution, due to the delay between stimulus and response, which varies up to 6 seconds. FMRI represents an indirect measure of brain activity, since the changes in signal intensity during the experiments reveal only the haemodynamic response of brain regions which are supposed to be involved in the perception or response to certain stimuli.

EEG is a direct measure of neuronal activity, and provides an effective means of measuring neuronal firing. It requires the synchronous activity of a large number of neurons to generate measurable electric potentials, and has the intrinsic problem of source localization uncertainty caused mostly by the skull. EEG signals are most likely derived from compact regions of cortex whose local field activities at the neuronal scale are similarly oriented by cortical geometry and partially synchronized, thereby producing signals that reach the scalp by volume conduction. In other words, the electric potentials generated in a brain region must travel a path through brain tissue, meningeal membranes, cerebrospinal fluid, bone, subcutaneous tissue and skin, resulting in loss of accuracy in detection of the signal source. Therefore, simultaneous EEG-fMRI, as a multimodal technique, has gained attention providing improved temporal and spatial resolution. It has been suggested that the BOLD signal is governed by local field potentials (Logothetis et al., 2001), which are also regarded to be

the basis of neuronal signalling assessed by EEG. Musall et al. (2012) demonstrated that neural synchrony can modulate EEG signals independently of amplitude changes in neural activity . Nevertheless, the exact mechanism of coupling between the haemodynamic response measured by BOLD/fMRI and the underlying neuronal activity is poorly understood and is still an area of intense discussion (Fox and Raichle, 1986; Malonek and Grinvald, 1996; Malonek et al., 1997; Heeger and Rees, 2002).

The fundamental assumption of any integration approach is that the signals recorded in both modalities are produced by closely interacting, or at least partly overlapping, brain structures. EEG is a selective measure of current source activity, whereas the haemodynamic fMRI signal is related to energy consumption of neural populations. Simultaneous acquisition of EEG and fMRI is recognized as a combination of complementary techniques, and gives rise to the question about the best method to achieve the integration during data analysis. Recent developments in simultaneous measurement allow EEG-informed single-trial analysis of the fMRI data. This is particularly important in studies where variability in responses may be indicative of stimulus processing modulation (Debener et al., 2005; Eichele et al., 2005; Bagshaw and Warbrick, 2007; Ostwald et al., 2010). An approach by Ostwald et al. (2010) with visual evoked potentials showed the success of using the properties of the EEG signal to predict changes in the BOLD response in the statistical framework of the general linear model (GLM). This is the so-called ‘integration by prediction’, where typically some feature from the EEG (e.g. alpha power, P300

amplitude) is convolved with a canonical haemodynamic response function and used as a predictor of haemodynamic activity in a GLM. Integration-by-prediction is based on the assumption that the haemodynamic response is linearly related to local changes in neuronal activity, particularly in local field potentials (Logothetis et al., 2001; Heeger and Ress, 2002; Lauritzen and Gold, 2003). In a study by Juckel et al., (2012) the P300 amplitudes were used in an EEG-fMRI joint analysis for the investigation of the age effects on P300. This approach proved to be successful in finding specific P300-related BOLD responses in the functional data analysis.

An important disadvantage of combining EEG and fMRI is, however, the highly contaminated EEG signal when it is acquired in the MR scanner environment. In the first place, gradient artefacts occur due to switching magnetic fields during fMRI acquisition. However, due to the consistency of this artefact over time, the subtracting methods such as average artefact template (Allen et al., 2000) are quite successful. A bigger challenge is posed by the ballistocardiogram (BCG) artefact, which is produced by cardiac pulse-related movement of the scalp electrodes inside the magnetic field. The precise source of the BCG artefact is unclear but it is related to a number of factors including pulsatile blood movement, small head movements and scalp expansion. The ballistic effect is thought to be due to motion induced in the body of the subject as blood is pumped upwards. Movement of electrically conductive material in a magnetic field results in electromagnetic induction; as such the motion related to cardiac activity can lead to electromotive forces in the circuit between the



subject and the recording equipment, thus resulting in additional artefacts in the recording. In addition to this ballistic effect there is also a pulse related artefact due to the Hall-effect, where small voltages are induced by the abrupt changes in blood flow velocity in proximity to the electrodes (Debener et al., 2008).

The correction of the BCG artefact is an essential step in order to retrieve valuable data when EEG is recorded simultaneously with fMRI. A number of techniques have been proposed to suppress the BCG artefact. One of the most widely accepted are optimal basis set (OBS, Niazy et al., 2005) and average artefact subtraction (AAS, Allen et al., 1998). Independent component analysis (ICA) was also suggested as a tool with high potential for removing artefacts in the EEG recordings (Jung et al., 2000).

## **1.2 Auditory evoked potentials and their clinical significance**

Auditory evoked potentials (AEPs) are a subclass of event-related potentials (ERPs). ERPs are defined as brain responses which are time-locked to some event, such as a sensory stimulus. The averaged ERPs are thought to be originated by synchronous activity in pyramidal cells in the activated areas and are easily measured by EEG. Due to the fact that volume conduction through the cerebrospinal fluid, skull, and scalp is thought to be linear, sensory ERPs are assumed to sum stable potentials associated with activation in each stimulated area (Makeig et al., 1997). The ERPs result mainly from the summation of cortical excitatory and inhibitory post-synaptic potentials

triggered by the release of neurotransmitters such as GABA and glutamate into the synaptic cleft (Mitzdorf, 1994). Recent neurophysiological evidence supports the notion that the features of the ERPs result from activity in several cortical sources that are intrinsically connected (Makeig et al., 2004).

The loudness dependence of auditory evoked potentials (LDAEP) is defined as the change in amplitude of the evoked potentials in response to various auditory stimulus intensities (Rapin et al., 1966), and is considered as a measure of serotonergic activity (Hegerl and Juckel, 1993; Hegerl and Juckel, 1994; Juckel et al., 1996; Hegerl et al., 2001). When the stimulus intensity increases, the individuals respond with a marked increase in the P1/N1 or N1/P2 component. Literature suggests that a pronounced LDAEP of the N1/P2 components reflects low central serotonergic neurotransmission (Hegerl and Juckel, 1993). Moreover, it is believed that the intensity of the AEPs is modulated by the serotonergic innervation of the auditory cortex and is useful as a reliable indicator of central serotonergic functions in humans. The inverse relationship between the LDAEP and the central serotonergic activity has been demonstrated by different methods and in different psychiatric disorders (Hensch et al., 2008; O'Neill et al., 2008a). Hegerl and Juckel (2000) found a significant relationship between strong LDAEP, indicating low serotonergic function, and a favourable response to selective serotonin reuptake inhibitors (SSRI) in depressed patients.

It has been extensively demonstrated that disturbances in the serotonergic system are present in various psychiatric syndromes

such as depression, obsessive-compulsive behaviour and generalized anxiety disorder. A better understanding of the serotonergic system and its modulation will be of great value in the design of better treatment strategies in the future. For example, a number of studies in patients with affective disorders show that a strong LDAEP serve as a predictor of favourable treatment response (Hegerl et al., 1992; Hegerl et al., 2001).

Different strategies have been used to determine the LDAEP. Dipole source analysis (DSA) and single electrode approaches are the most often used methods. The DSA permits the localisation of the main neuronal generators in the cortex by estimating intracerebral sources for surface scalp-recorded waveforms (Scherg et al., 1989). In human studies this can indirectly be achieved by using multichannel-EEG with additional source analysis (Scherg and Von Cramon, 1986; Gallinat and Hegerl, 1994). The DSA is a technique that allows the separation of the auditory evoked N1/P2 components into subcomponents generated by the primary and secondary auditory cortices. It has been suggested that the LDAEP generated by the primary and secondary auditory cortices may be isolated and analyzed separately using DSA (Hegerl and Juckel, 1993; Gallinat and Hegerl, 1994; Norra et al., 2008). Multichannel-EEG and DSA require special expertise and have been considered to be extremely time-consuming (Hensch et al., 2008). Thus, many studies use only one or a few EEG channels at central sites, mostly Cz, to determine the LDAEP (Lee et al., 2005; Kawohl et al., 2008; O'Neill et al., 2008b). The Cz channel has been reported to be the best single electrode position for assessing

activity of the auditory cortices if multichannel based DSA is unavailable (Hensch et al., 2008).

A number of studies have shown that the change in amplitude of the AEPs is positively correlated with a growth in the cortical response (Hegerl et al., 1994; Dierks et al., 1999; Brocke et al., 2000; Mulert et al., 2005). In a study by Mulert et al., (2005) during a simultaneous 61-channel EEG and fMRI measurement, a high correlation between the loudness-dependent change of the extent of fMRI activation and the corresponding changes of the mean current source density within the same region of interest covering the primary auditory cortex (PAC) was found.

Nevertheless, and despite numerous investigations, the exact brain regions implicated in the processing of rising sound pressure levels remain unclear. Importantly, an increased N1/P2 amplitude would imply an enlarged cortical response that might not be limited to the PAC. The aforementioned integration by prediction method of analysing simultaneous EEG data would provide additional and more detailed information on the cortical processing of high sound pressure levels.

### **1.3 Integrating the ERP information into the LDAEP fMRI data analysis**

Although the loudness dependence of cortical response has been demonstrated separately in EEG and fMRI experiments, the integration of the two techniques into a unique analysis of data recorded during an LDAEP paradigm has never been accomplished. This leads to the question of which of the EEG parameters

correlates with the extent or strength of the activation in the fMRI data. On the basis of the positive correlation between amplitude of the AEPs and extent of the BOLD signal in the primary auditory cortex demonstrated by Mulert et al. (2005), we hypothesize that including the N1/P2 individual amplitudes into the fMRI analysis will show additional activated voxels which will explain the inter-subject and loudness intensity variability. Thus, these analyses are expected to show the cortical structures engaged in auditory perception and processing of rising sound pressure levels. In this regard, an increased engagement of the insular cortex in auditory perception at higher sound pressure levels is also expected and thus, the insular cortex is expected to be involved in the generation of the LDAEP. Some studies have discovered new roles for the insula, suggesting it as a somatosensory area and emphasizing its multifaceted sensory role (Augustine 1996). There is also evidence that the insular cortex is involved in sound detection and entry of the sound into awareness (Engelien et al., 1995; Downar et al., 2000; Kiehl et al., 2001).

#### **1.4 Hypotheses**

Based on the currently available evidence we hypothesize that other cortical regions apart from the PAC are implicated in the cortical response that occurs with tones of different intensities. We also hypothesize that such structures play a role in the amplitude variability of the AEPs that can be measured from the scalp during and LDAEP paradigm.

The intention of this study is to answer the following questions through a simultaneous EEG-fMRI measurement:

- Does the integration of the N1/P2 amplitudes into the fMRI analysis result in an extended map of the brain responses during an LDAEP paradigm in comparison to an 'uninformed' fMRI analysis?
- Which other brain regions are involved in the processing of rising sound pressure levels?
- Which differences can be observed in the brain response to low and high intensity tones?
- Is the insular cortex engaged in the processing of rising sound pressure levels?

The secondary aim of this study is to explore different methods, such as ANOVA of fMRI data, for the investigation of the structures involved in the generation of the LDAEP.

## 2 Methods

### 2.1 Subjects and measurements

During a single session measurement, EEG was recorded simultaneously with fMRI using MR compatible devices from 16 healthy volunteers (10 males, 6 females, mean age = 31.06 years old, SD = 8.90). Written informed consent was obtained from all subjects and the study was approved by the Ethics Committee of the Medical Faculty of the Rheinisch-Westfälische Technische Hochschule Aachen (RWTH Aachen University). The study was conducted according to the Declaration of Helsinki.

EEG data were recorded in Brain Vision Recorder (Version 1.20, Brain Products, Gilching, Germany) using a 64-channel MR compatible EEG system including an MR compatible amplifier and a synchronisation box (Brain Products, Gilching, Germany). The EEG cap (BrainCap MR, EasyCap GmbH, Breitbrunn, Germany) consisted of 63 scalp electrodes distributed according to the 10-10 system and one additional electrode for recording the electrocardiogram (ECG) (Figure 1). Data were recorded relative to a Fpz reference and a ground electrode was located at AFz (10-5 electrode system, Oostenveld and Praamstra, 2001). Data were sampled at 5000 Hz, with a bandpass of 0.016 – 250 Hz. Impedances at all recording electrodes were kept below 10 k $\Omega$ .

FMRI data were recorded in a 3T Siemens Magnetom Tim-Trio MR scanner. For functional BOLD imaging, a T2\*-weighted EPI sequence was used (TR = 2.2 s, TE = 30 ms, field-of-view = 200

mm, slice thickness = 3 mm and number of slices = 36). The functional time series consisted of 1670 volumes, the total duration of the fMRI measurement was 61.2 minutes. Anatomical images were acquired for every subject by means of a Magnetisation-Prepared, Rapid Acquisition Gradient-Echo (MP-RAGE) sequence (TR = 2250 ms, TE = 3.03 ms, field-of-view =  $256 \times 256 \times 176$  mm<sup>3</sup>, matrix size =  $256 \times 256$ , flip angle =  $9^\circ$ , 176 sagittal slices with 1 mm slice thickness and a GRAPPA factor of 2 with 70 autocalibration signal lines).

The subjects were requested to lie down and relax during the measurement. A 'Mr. Bean' video was presented during the recording as a distraction. Four hundred tones with a frequency of 1 kHz, a duration of 40 ms but with different sound pressure levels were presented using Presentation software (Neurobehavioral Systems, Inc, Albany, US). The sound pressure levels of the tones were 70, 80, 90 and 100 dB. The timing and order of the tones were randomized using optseq2 (<http://www.freesurfer.net/optseq/>). Optseq is a tool for automatically scheduling events for rapid-presentation event-related fMRI experiments. It permits that more stimuli can be presented within a given scanning interval at the cost of assuming that the overlap in the haemodynamic responses will be linear. The resulting ISI varied between 6.62 – 19.83 s.

There was a delay of 26 ms between the stimuli marker in the EEG recording and the actual presenting of the tones to the volunteers. The delay between the EEG marker and the tones was measured via oscilloscope by establishing the time between the marker



signal and the onset of the tones. This time was constant and was due to processing times in the sound card of the stimulation computer.

## **2.2 EEG data analysis**

The EEG data were processed using Brain Vision Analyzer (Version 2.0. Brain Products, Munich, Germany). Gradient correction was performed using the method proposed by Allen et al. (2000) and included in Brain Vision Analyzer. Down-sampling to 250 Hz and a low-pass filter with a cut-off frequency of 40 Hz were applied. Further filtering was applied to the data, using an infinite impulse response (IIR) filter with a low cut-off of 0.16 Hz and a high cut-off of 20 Hz; a notch filter was not applied. The data were later re-referenced to an average reference. For correction of the ballistocardiogram (BCG) artefact the pulse events were first detected and marked in the ECG channel, where a pulse template was sought between 0 and 10 s. The detection method was carried out in semi-automatic mode, where non-detected heartbeat events were visually identified and marked. The artefact subtraction was carried out using the method proposed by Allen et al. (1998) included as toolbox in Brain Vision Analyzer, where the time delay was automatically estimated over the whole data set. The EEG data were later segmented around the event markers, 100 ms before the onset time and 500 ms after. Segments with residual artefacts were automatically excluded using the following amplitude parameters: minimal allowed amplitude of  $-80\text{ }\mu\text{V}$ , maximal allowed amplitude of  $80\text{ }\mu\text{V}$ . The non-excluded segments were later averaged. Two peaks were

detected and visually confirmed in semiautomatic mode at Cz channel: N1 (negative polarity and latency between 100 and 180 ms) and P2 (positive polarity and latency between 190 ms and 275 ms). For the detection of the peaks, the delay between the marker and the presentation of the stimuli was taken into account. The amplitudes and latencies at individual level were exported for statistical analysis and construction of covariants for the fMRI analysis.

### 2.2.1 Determination of the LDAEP

The median slope of the amplitude-intensity function of LDAEP was calculated from the slopes of all possible connections over the four sound pressure levels (70, 80, 90 and 100 dB) according to the following formula (Hegerl & Juckel, 1994):

$$LDAEP = \frac{70 p_{70dB} + 80 p_{80dB} + 90 p_{90dB} + 100 p_{100dB} - 4 \mu_{(70dB-100dB)} \mu_{p(70dB-100dB)}}{70^2 + 80^2 + 90^2 + 100^2 - 4 \mu_{(70dB-100dB)}^2}$$

Where  $p_n$  are the N1/P2 amplitudes (Cz channel) at each sound intensity,  $\mu_{(70dB-100dB)}$  is the mean of sound intensities and  $\mu_{p(70dB-100dB)}$  is the mean of N1/P2 amplitudes at each sound intensity.

## 2.3 fMRI data analysis

### 2.3.1 Single-level analysis

Functional data were analysed using FMRI Expert Analysis Tool (FEAT), included in FSL (Version 5.0.4. FMRIB's Software Library, <http://fsl.fmrib.ox.ac.uk/fsl/fslwiki/FEAT>). Individual pre-processing consisted of motion correction using MCFLIRT (Jenkinson et al., 2002), brain extraction using BET (Smith 2002), spatial smoothing using a Gaussian kernel of full-width at half maximum (FWHM) of 5 mm, and high-pass temporal filtering with a period of 100 s. FMRI volumes were registered to the structural scan of the individuals and also to a standard space (MNI152) using FMRIB's Nonlinear Image Registration. Z (Gaussianised T/F) statistic images were thresholded using clusters determined by  $Z > 2.3$  and a (corrected) cluster significance threshold of  $p \leq 0.05$ . The subject-level model included 4 regressors, one for every type of stimulus (tone intensity), and double gamma-HRF as convolution. The GLM model included contrasts to obtain the mean of each stimulus type: 70 dB (1 0 0 0), 80 dB (0 1 0 0), 90 dB (0 0 1 0) and 100 dB (0 0 0 1) for each individual subject. Motion parameters were included in the model in order to correct for additional motion artefacts.

Motion parameters of the single-level analysis are presented in Appendix I.

### *2.3.2 Higher-level analysis*

A higher-level analysis was carried out using FLAME (FMRIB's Local Analysis of Mixed Effects) stage 1 and stage 2 (Beckmann et al., 2003; Woolrich, 2008; Woolrich et al., 2004). The first level contrasts described above were included in the GLM model. In addition the N1/P2 amplitudes were included as covariants in order to

explain activation related to inter-subject BOLD signal variation with the four sound pressure levels as follows: mean group effect at 70 dB (1 0 0 0 0 0 0 0) and N1/P2 at 70 dB (0 1 0 0 0 0 0 0), mean group effects at 80 dB (0 0 1 0 0 0 0 0) and N1/P2 at 80 dB (0 0 0 1 0 0 0 0), mean group effects at 90 dB (0 0 0 0 1 0 0 0) and N1/P2 at 90 dB (0 0 0 0 0 1 0 0), mean group effects at 100 dB (0 0 0 0 0 0 1 0) and N1/P2 at 100 dB (0 0 0 0 0 0 0 1). Thus, two contrasts were obtained for each sound intensity, one containing the mean activation of the group and the other containing the covariant influence on the group. Statistic images were thresholded using clusters determined by  $Z > 2.0$  and a corrected cluster significance threshold of  $p \leq 0.05$ . For the comparison of low (70 and 80 dB) and high (90 and 100 dB) intensity tones two additional contrasts were calculated: an EEG-informed analyses of low  $>$  high (1 1 1 1 -1 -1 -1 -1) and high  $>$  low (-1 -1 -1 -1 1 1 1 1).

### 2.3.3 Repeated measures ANOVA

An alternative repeated measures analysis of variance (ANOVA) was also performed across subjects in order to investigate brain regions involved in the variability of responses to the different sound pressure levels. The model included 1 factor (tones) at 4 levels (70, 80, 90 and 100 dB). The contrasts included were those generated by the fMRI single-level analysis. The calculation of the ANOVA was carried out using FLAME stage 1 (Beckmann et al., 2003; Woolrich, 2008; Woolrich et al., 2004). Statistic images were thresholded using clusters determined by  $Z > 2.3$  and a corrected cluster significance threshold of  $p \leq 0.05$ .

#### *2.3.4 Region of Interest analysis*

In order to perform a region-of-interest (ROI) analysis, masks of ROIs were also created in FSLVIEW (FMRIB's Software Library, <http://fsl.fmrib.ox.ac.uk/fsl/fslview/>) using the Harvard-Oxford cortical structural atlas (Harvard Center for Morphometric Analysis, Massachusetts, US). The ROIs were those structures involved in sound perception, as well as the neighbouring areas and some frontal sources described in the literature (Angrilli et al., 2008). The selected ROIs were the following: anterior cingulate cortex (ACC), medial frontal cortex (MFC), Heschl's gyri, bilateral insular cortices, bilateral orbito-frontal cortices (OFC), and frontal operculum (Figure 3). The number of activated voxels within ROIs was extracted from the contrasts generated by the higher-level analysis using the `'fslstats'` script (FSLUTILS, <http://fsl.fmrib.ox.ac.uk/fsl/fslwiki/Fslutils>).

## **3 Results**

### **3.1 EEG data analysis**

#### *3.1.1 Auditory evoked potentials*

The EEG data were successfully corrected for gradient and BCG artefacts and the trial-average showed clear AEPs for the four sound pressure levels (Figure 4). Descriptive statistics of the ERPs at each sound pressure level are summarized in Table 1. The mean N1/P2 amplitude of the tones at 70 dB was 2.16  $\mu$ V (SD = 1.84), at 80 dB was 4.53  $\mu$ V (SD = 2.72), at 90 dB was 6.86  $\mu$ V (SD = 3.59) and at 100 dB was 11.26  $\mu$ V (SD = 4.21). Increasing amplitudes were observed at higher sound pressure levels, proving that the stimulation paradigm was successful in exhibiting LDAEP.

#### *3.1.2 LDAEP calculation*

The LDAEP was calculated for each subject including the N1/P2 amplitudes according to the formula of Hegerl and Juckel (Hegerl & Juckel, 1994). The mean LDAEP of the group was 0.30  $\mu$ V/10dB (SD = 0.11).

### **3.2 Functional data analysis**

#### *3.2.1 Higher-level analysis of the functional data*

The structures which exhibited consistent activation with the

four sound pressure levels were the angular gyri, central opercular cortices, frontal operculum cortices, Heschl's gyri, insular cortices, middle temporal gyri, parietal operculum cortices, planum polare, bilateral planum temporale, postcentral gyri, precentral gyri, superior temporal gyri, temporal pole and putamen bilaterally.

The analysis of fMRI data showed growth in the cortical response of the PAC with increasing sound pressure levels. In addition to the structures activated with the 70 dB stimuli (Figure 5), the 80 dB stimuli elicited activation in the right amygdala, right frontal orbital cortex, right pallidum, left superior parietal lobule and right thalamus (Figure 6). The 90 dB stimuli elicited additional activation in the caudate, right ACC, posterior cingulate cortices, frontal pole bilaterally, hippocampus, lateral occipital cortices, lingual gyri, middle frontal gyri and the parahippocampal gyri (Figure 7). The 100 dB stimuli elicited additional activation in the nucleus accumbens, cuneal cortices, frontal medial cortices, right inferior temporal gyrus, intracalcarine cortices, supplementary motor cortices, occipital fusiform cortices, occipital pole, paracingulate gyri, precuneus, superior frontal gyri, supracalcarine cortices, left temporal fusiform cortex and temporal occipital fusiform cortices (Figure 8). Clusters of maximum with the 70, 80, 90 and 100 dB tones in the fMRI data analysis are presented in Tables 2, 3, 4 and 5 respectively.

### *3.2.2 Inclusion of the AEPs amplitudes into the fMRI analysis*

Integrating N1/P2 amplitudes into the analysis the fMRI data resulted in voxel-wise maps showing clusters where the z-scores covaried with the N1/P2 amplitudes in an inter-subject level.

The contrasts holding N1/P2 information exhibited consistent covariation across the four tones in the right central opercular cortices, right frontal operculum cortices, right frontal orbital cortices, right Heschl's gyrus, right inferior frontal gyrus, right insular cortex, right parietal operculum cortex, right planum polare, right planum temporale, right postcentral gyrus, right precentral gyrus, right putamen, right superior temporal gyrus and right temporal pole.

In addition to the structures revealed by the group analysis of the fMRI data, the covariate contrast of the 70 dB stimuli revealed additional activation in the right orbital cortex and right pallidum (Figure 9). The covariate contrast with of the 80 dB stimuli added the left caudate, pars triangularis of the right inferior frontal gyrus and right parahippocampal gyrus (Figure 10). The covariate contrast of the 90 dB stimuli added the nuclei accumbens, cuneal cortices, right inferior temporal gyrus, intracalcarine cortices, supplementary motor cortices, occipital fusiform gyri, occipital pole, paracingulate gyri, precuneus cortices, superior frontal gyri, supracalcarine cortices and temporal fusiform cortices (Figure 11). Surprisingly when the N1/P2 amplitudes of the 100 dB tones were included into the fMRI analysis, most of the voxels which exhibited covariation were those located in the primary visual cortex (PVC), and there-



fore the covariate contrast did not provide additional information (Figure 12).

Clusters with maximal covariance with N1/P2 amplitudes at 70, 80, 90 and 100 dB are presented in Tables 6, 7, 8 and 9 respectively. A complete list of the structures which exhibited activation with the four tones is presented in Table 10.

### *3.2.3 ROI analysis*

The ROI analysis of activated voxels within Heschl's gyri and other regions showed a greater number of voxels in the EEG-informed fMRI analysis when compared to the fMRI alone analysis (Table 11). A paired t-test revealed this difference as statistically significant:  $t(23) = -3.471$ ,  $p = 0.02$ . The analysis showed increasing activation in the Heschl's gyri and insular cortices with increasing sound pressure levels. The EEG-informed analysis also revealed a number of activated voxels in frontal regions such as the opercular cortices, OFC and ACC, particularly significant with the 90 and 100 dB stimuli. This was not the case for the MFC, which did not exhibit significant activation with any of the stimuli (Figure 13).

### *3.2.4 Repeated measures ANOVA*

The ANOVA of 1 factor at 4 levels exhibited brain regions whose BOLD response presented consistent variability with the different tone intensities (Figure 14). The areas which exhibited consisted variation as revealed by the ANOVA were the Heschl's gyri (includes H1 and H2), planum temporal bilaterally, parietal operculum cortices, central opercular cortices, posterior cingulate cortex and

the ACC. See Table 12.

### *3.2.5 Comparison of High and Low intensity tones*

The inclusion of the N1/P2 amplitudes resulted in an extended activation map that revealed different areas involved in the response to the tones. The voxel-wise statistical maps which resulted from the comparison of low (70 and 80 dB) and high (90 and 100 dB) intensity tones exhibited significant differences ( $p < 0.05$ ). The high intensity tones showed significant additional activation in the right and left Heschl's gyri, right and left insular cortices, right and left planum polare, right posterior cingulate cortex, left supra-marginal gyrus, left cuneal cortex, right frontal operculum cortex, right OFC, right and left lateral occipital cortices, right and left angular gyri, left middle frontal gyrus, right postcentral gyrus and the right middle temporal gyrus (Figure 15). See Table 13. The low intensity tones did not exhibit any significant additional activation in comparison to the high intensity tones.

## 4 Discussion

### 4.1 Effectiveness of the auditory stimulation

The auditory paradigm used proved to be successful for both fMRI and EEG. The presented results show a change in amplitude of the auditory evoked potentials in response to the various auditory stimulus intensities (Rapin et al., 1966), confirming the existence of LDAEP in the data. The paradigm was successful in terms of identifying the growth in cortical activation with increasing sound pressure levels according to previous studies (Hegerl et al., 1994; Dierks et al., 1999; Brocke et al., 2000; Mulert et al., 2005).

### 4.2 Correlation between the AEP amplitudes and the extent of fMRI cortical response

The main reason to combine EEG and fMRI is the synergistic effect of combining the high temporal resolution of the electrophysiological measurements with the high spatial resolution of fMRI imaging (Blinowska et al. 2009; Debener and De Vos 2011; Debener and Herrmann 2008). The presented results showed that the EEG-informed fMRI analysis extended the brain activation map and uncovered voxels carrying valuable information that would have been hidden using fMRI alone. The statistical maps resulting from the inclusion of the ERP-amplitudes as covariates in the fMRI data analysis, illustrate the voxels where the BOLD signal fluctuations covaried with the N1/P2 amplitudes, and thus, had an influence on

the inter-subject variation of the response to stimuli. Integrating the ERP parameters as predictors in the functional data allows one to reveal additional brain areas that are also important in the response to the acoustic stimuli. In line with previous work (Mulert et al., 2005) this method introduces an effective way to find correlations between the cortical responses to auditory stimuli that could be detected by both AEPs and fMRI. These findings also support the coupling between the EEG and BOLD responses during auditory stimulation described by Mayhew et al. (2010).

### **4.3 Involvement of cortical structures in sounds perception and LDAEP**

The aim of this study was to identify the cortical structures contributing to the amplitude variation of the AEPs at different sound pressure levels. The data showed that the Heschl's gyri, as a marker of human PAC (Da Costa et al., 2011), were consistently activated during the paradigm at the 4 different sound pressure levels, and that the extent of cortical response was larger at high sound pressure levels. Other structures were also consistently activated by the stimuli, such as the angular gyri, central opercular cortices, frontal operculum cortices, insular cortices, middle temporal gyri, parietal operculum cortices, planum polare, bilateral planum temporale, postcentral gyri, precentral gyri, superior temporal gyri, temporal pole and the putamen. The constant presence of voxels in the Heschl's gyri whose signal covaried with the N1/P2 amplitudes enables one to assert that the main cortical structure engaged in the generation of the AEPs is the PAC. Therefore, the inter-subject variation

of the haemodynamic response to the stimuli explains the variation in amplitude that can be observed in the excitatory potentials that generate the scalp ERPs. In addition to this, the ROI analysis shows a regular pattern of increasing number of active voxels at higher sound pressure levels in the insular cortex.

The ANOVA pointed to the PAC, the posterior cingulate cortex and ACC as the structures which exhibited significant signal variation with increasing sound pressures (Figure 14), suggesting that such areas play an important role in the generation of the LDAEP. The higher-level analysis confirmed the latter, since additional activation was found in the PAC and right posterior cingulate cortex with the high intensity tones (90 and 100 dB).

Interestingly, the results of the ROI and higher-level analyses showed that the right and left insular cortices exhibit larger activation with high intensity tones. The insular cortex is a complex structure with several functions (for a review refer to Bamiou et al., 2003). The association of the insular cortex with sensory areas is well described (Augustine 1996); connections have been described between the insula and the orbital cortex, frontal operculum, lateral premotor cortex and ventral granular cortex. The insula also connects with the temporal pole and the superior temporal sulcus of the temporal lobe. There is evidence that insular cortices are involved in sound detection and entry of the sound into awareness (Engelien et al., 1995; Kiehl et al., 2001). In an fMRI study, Downar et al. (2000) described a multimodal network for involuntary attention to events in the sensory environment that includes the insular cortex. The results presented here add an important feature to

the functions of insular cortex i.e., engagement in auditory processing and also increasing response at high sound pressure levels. Although the response of insula might not be related to sound perception, it could be related to auditory stimuli processing, meaning that the increasing cortical response to the higher sound pressure levels is related to an intrinsically and involuntary attentional demand that is integrated in this area. The results presented here support the functions of the insula as a sensory and integrative area.

The OFC and ACC also appeared in the ROI analysis as structures that exhibited activation with high intensity tones. The prefrontal cortex, especially the OFC is one of the highest order associative cortical regions of the brain. Lesions of the dorsolateral prefrontal cortex are typically associated with a number of deficits in high level cognitive processes (Stuss and Benson, 1984). It was also demonstrated that patients with focal lesions of the OFC had a significant inhibition of the startle amplitude, together with a reduced self-evaluated perception of the unpleasantness of the acoustic probe stimulus (Angrilli et al., 2008). In a similar manner, the ACC has been described as part of a neural system dedicated to attention and orientation to danger, and also as an important part of the network that modulates startle responses (Pissioti et al., 2003).

Another interesting finding in the results presented here is the activation of the visual cortex particularly with the 90 and 100 dB tones. In this regard, that effect could be due to cross-modal effects induced by the distracting video. The results presented here showed increased cross-modal effects at high sound pressures. Supporting

this assertion there is evidence of strong activation of the insular cortices in the results. In a PET study conducted by Buschara et al., (2001) it was demonstrated that the insular cortex mediates temporally defined auditory-visual interaction at an early stage of cortical processing. In a similar manner, Calvert et al. (2001) showed that the insular cortex exhibit cross-modal interactions when the subjects were exposed to synchronous and asynchronous auditory and visual stimuli. Thus, the results here suggest that the cross-modal effects of auditory-visual integration are stronger at high sound pressure levels and possibly that such integration is facilitated by the increased engagement of the insula.

#### **4.4 Limitations of the study**

One of the important limitations of the study was the duration of the paradigm (61 minutes). The length of the experiment made it highly susceptible to motion artefacts due to movements of the subject inside the scanner. This difficulty was addressed using a common used motion-correction method: MCFLIRT (Jenkinson et al., 2002). This method yielded satisfactory results (See Appendix I) and permitted a reliable analysis.

## **5 Conclusion**

The results presented here demonstrate that the extent of cortical activation involved in auditory processing rises along with rising sound pressure levels. There was activation of the ACC, the opercular cortices and of the OFC with high sound pressure levels. The PAC, posterior cingulate cortex and insular cortex exhibited involvement in the processing of rising sound pressure levels. Interestingly, a strong response of the visual cortex was also found at high sound pressure levels. We hypothesize that this is due to cross-modal effect of the tones in the visual cortex and that it was facilitated by the presentation of the distracting video via the integrative roles of the insula.

From a methodological point of view, our study supports the suitability of including the N1/P2 amplitudes extracted from the AEPs into the analysis of fMRI data in order to enrich the results.

It could also be demonstrated that the insular cortex plays an important role in the brain response to acoustic stimulation.



## **6 Acknowledgments**

The author thanks Dr. Irene Neuner for the research idea, the design of the study, the help during the acquisition of the data, the training and directions for the analysis and the corrections to the manuscript.

The author thanks Dr. Wolfram Kawohl for the research idea, the design of the study, the help during the acquisition of the data, the training and directions for the analysis and the corrections to the manuscript.

The support from Dr. Konrad Hitz and Ms. Christine Wyss during the acquisition of the data is gratefully acknowledged as well as their corrections to the manuscript.

The author would like to thank Dr. Tracy Warbrick for guidance during the analysis process as well as her corrections to the manuscript.

The author thanks Dipl.-Ing. Frank Boers for the setting of the stimulation paradigm, necessary for the acquisition of the data.

The author thanks Prof. N. Jon Shah for the research idea, the design of the study, the corrections to the manuscript and the supervision during the entire research process.

## 7 Figures



*Fig. 1: MR compatible EEG cap*  
*Source: Own creation*

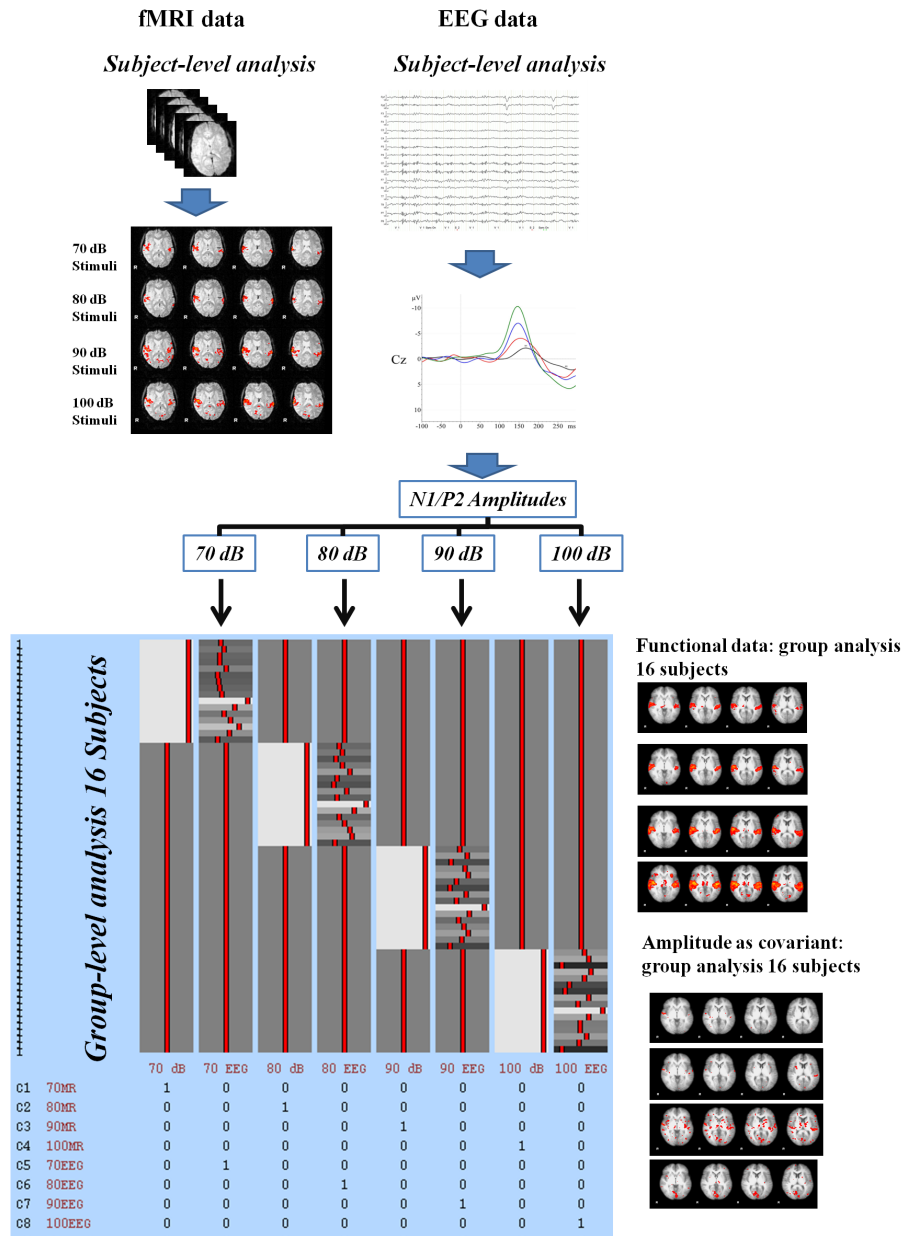


**Fig. 2: Methodological approach for fMRI data analysis**  
Source: Own creation

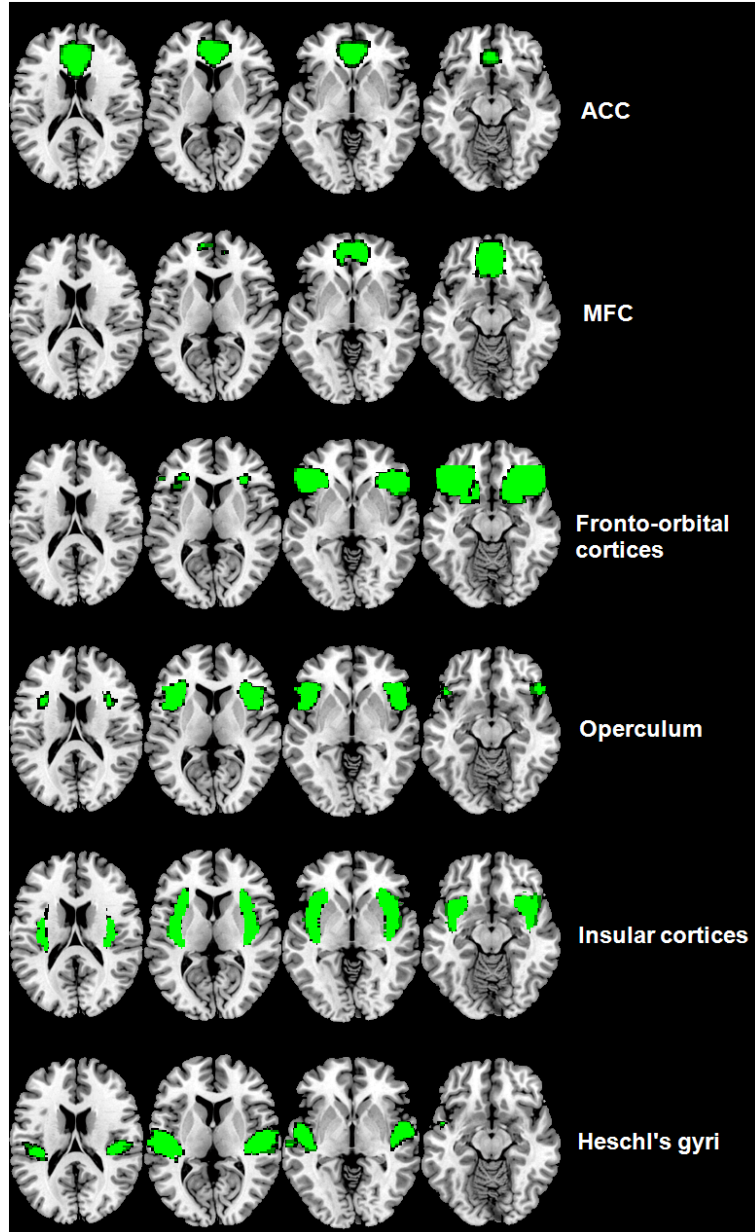


*Fig. 3: Masks of the regions of interest (ROI) created according to the Harvard-Oxford cortical structural atlas*  
*Source: Own creation*

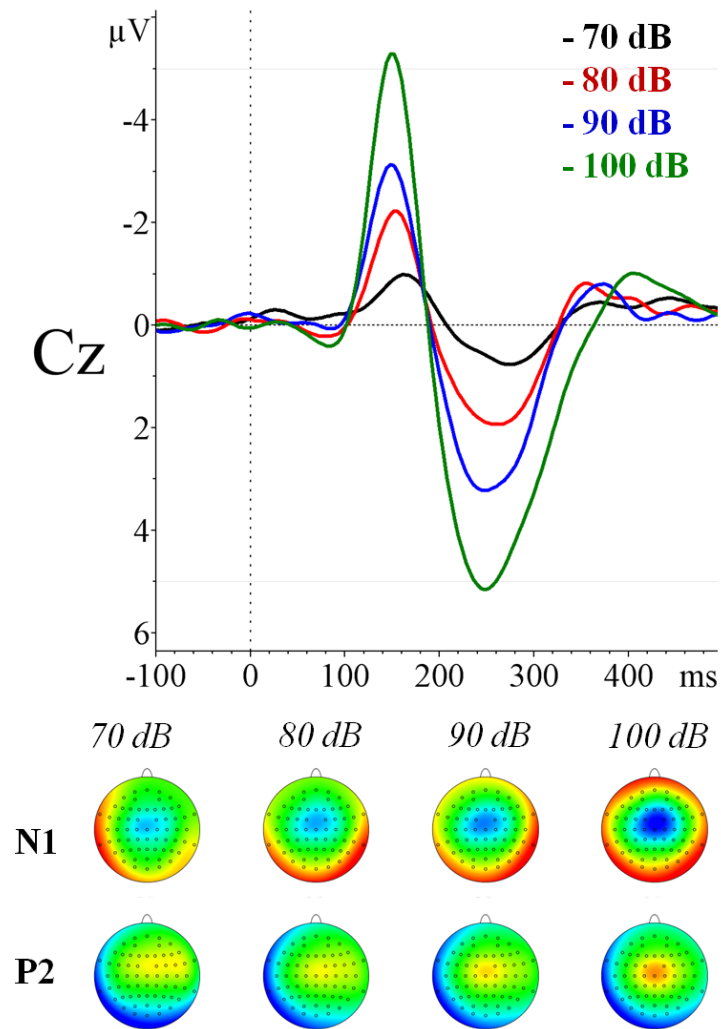


*Fig. 4: Grand average ( $n = 16$ ) of the auditory evoked related potentials for the different sound pressure levels at Cz measured inside the scanner.*

*Source: Own creation*

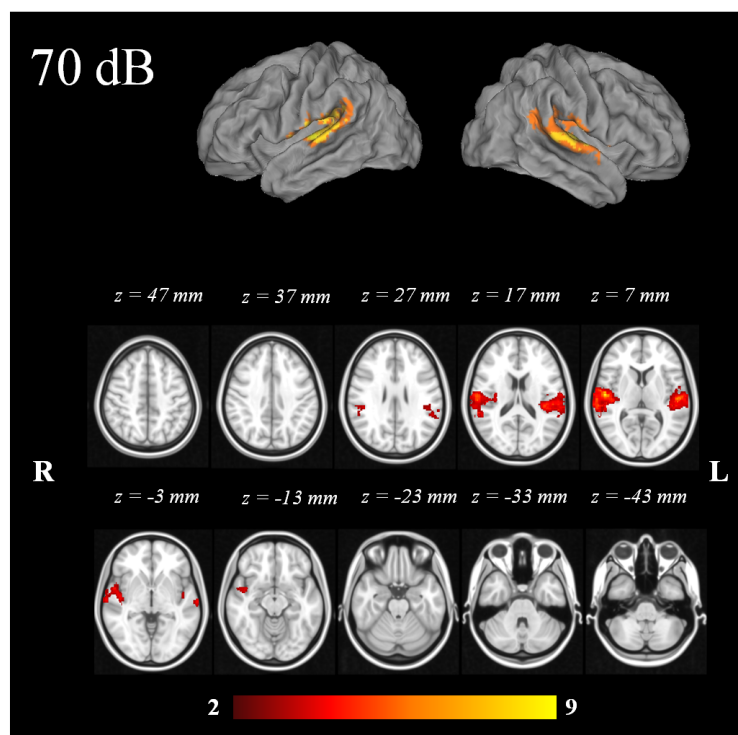


*Fig. 5: Mixed effects group analysis ( $n = 16$ ) of the fMRI activation related to the 70 dB stimuli*  
*Source: Own creation*

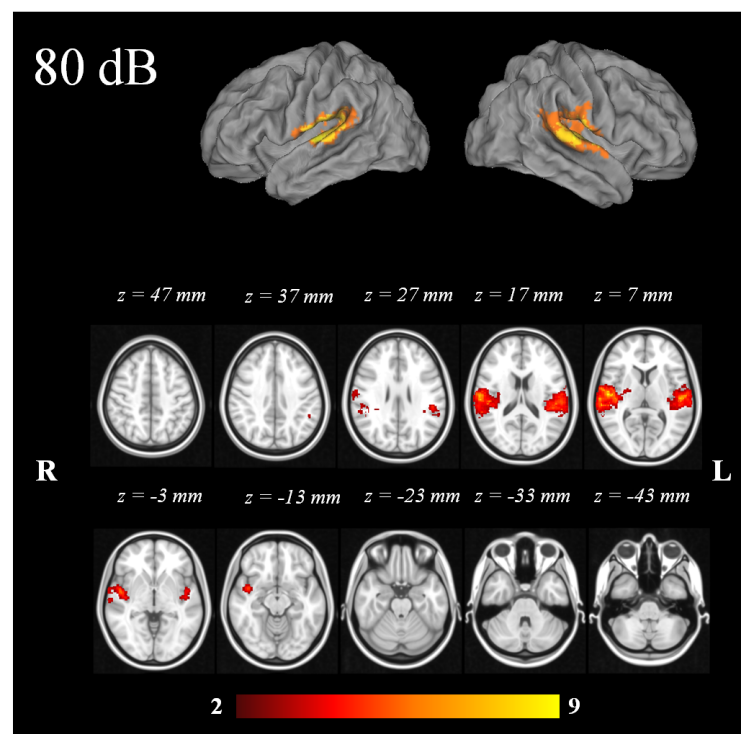


*Fig. 6: Mixed effects group analysis ( $n = 16$ ) of the fMRI activation related to the 80 dB stimuli*  
*Source: Own creation*

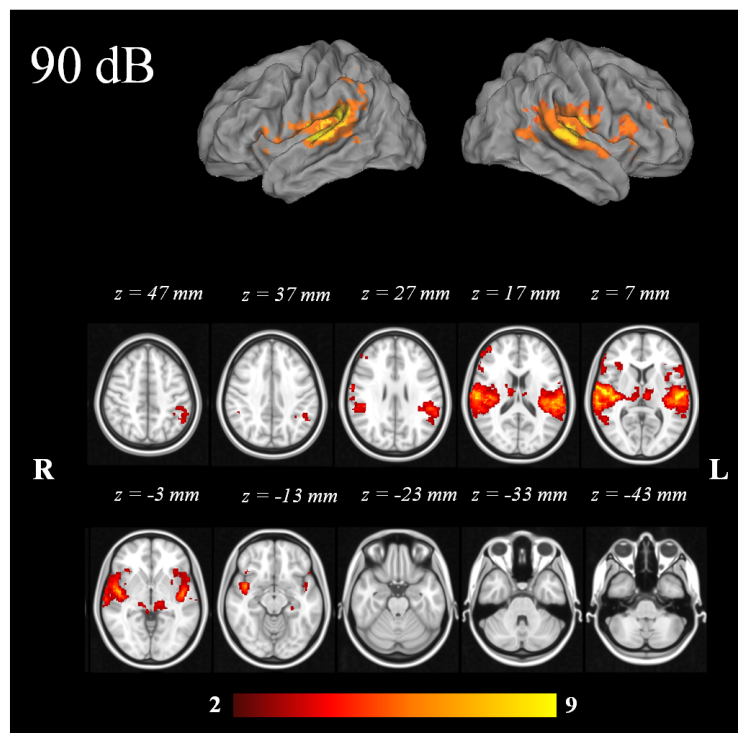


*Fig. 7: Mixed effects group analysis ( $n = 16$ ) of the fMRI activation related to the 90 dB stimuli*  
*Source: Own creation*



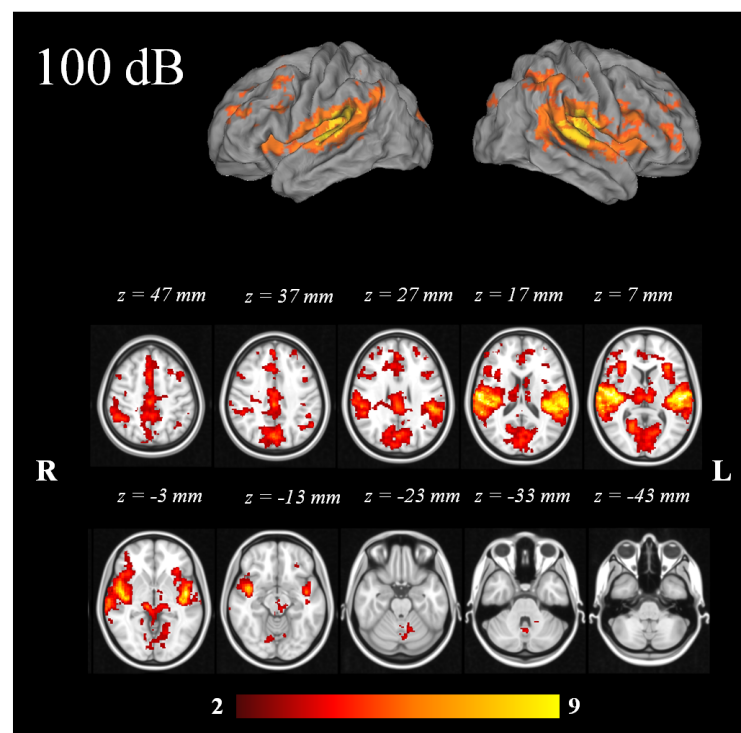


**Fig. 8:** Mixed effects group analysis ( $n = 16$ ) of the fMRI activation related to the 100 dB stimuli  
Source: Own creation

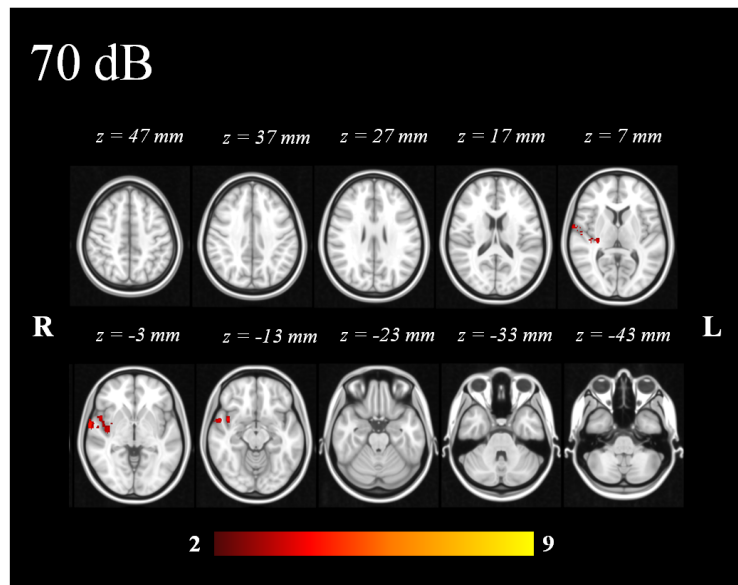


*Fig. 9: Voxel-wise statistical map of the significant clusters showing covariance with N1/P2 amplitudes at 70 dB.  
Source: Own creation*

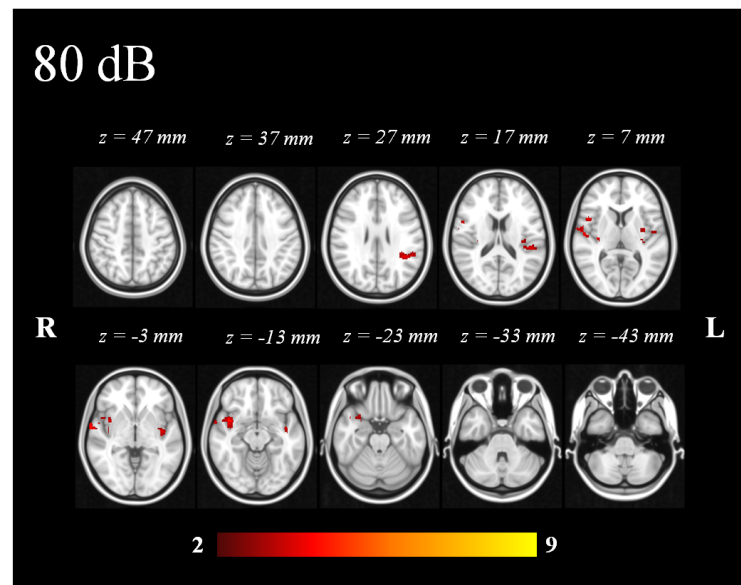


*Fig. 10: Voxel-wise statistical map of the significant clusters showing covariance with N1/P2 amplitudes at 80 dB.*

*Source: Own creation*

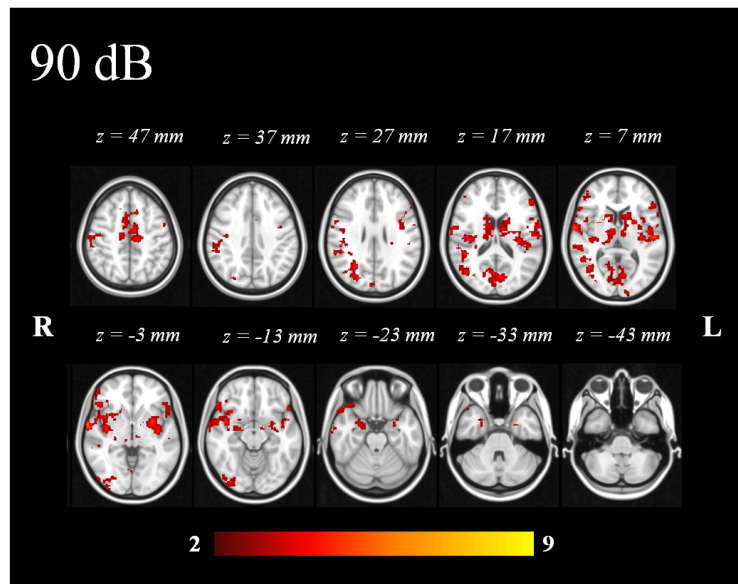


*Fig. 11: Voxel-wise statistical map of the significant clusters showing covariance with N1/P2 amplitudes at 90 dB.*

*Source: Own creation*

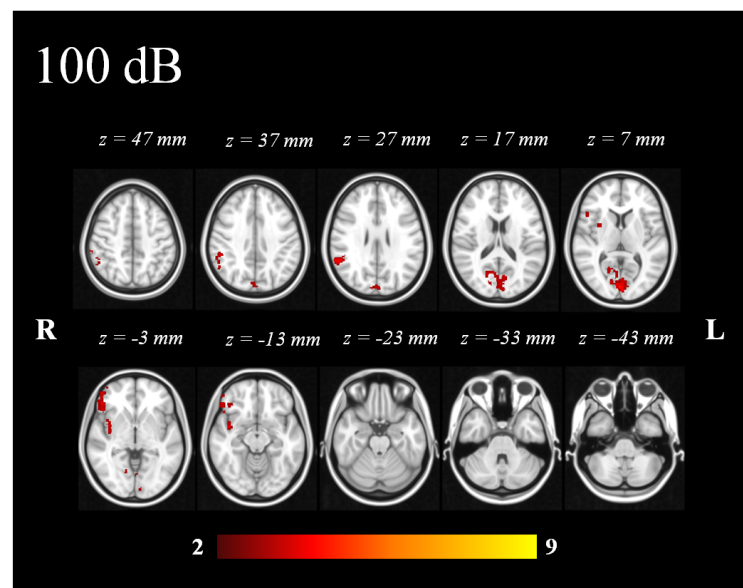


*Fig. 12: Voxel-wise statistical map of the significant clusters showing covariance with N1/P2 amplitudes at 100 dB.*  
*Source: Own creation*

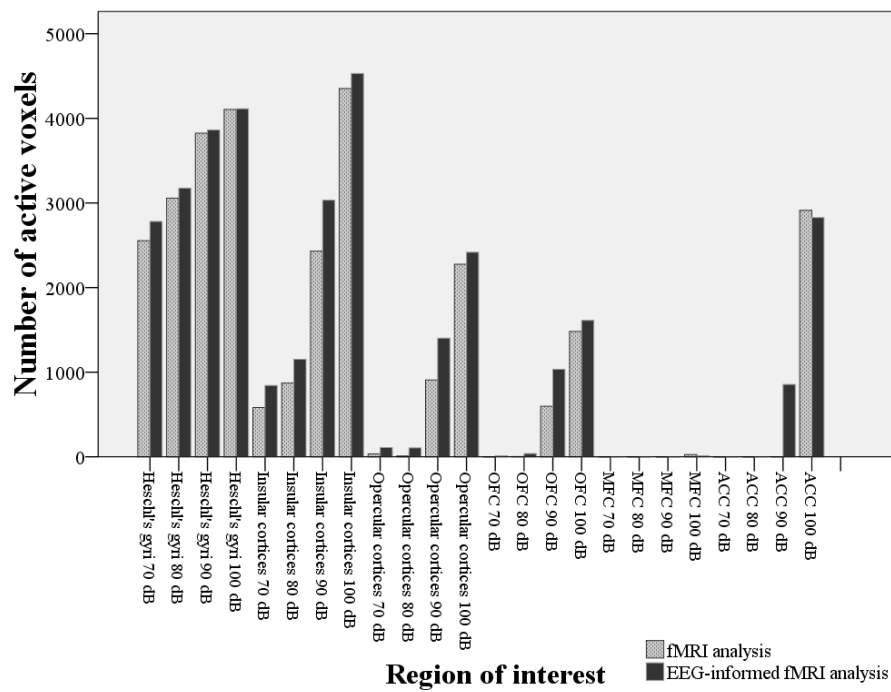


**Fig. 13:** Number of activated voxels within the ROI at each sound pressure for fMRI alone analysis and EEG-informed fMRI analysis.

Source: Own creation

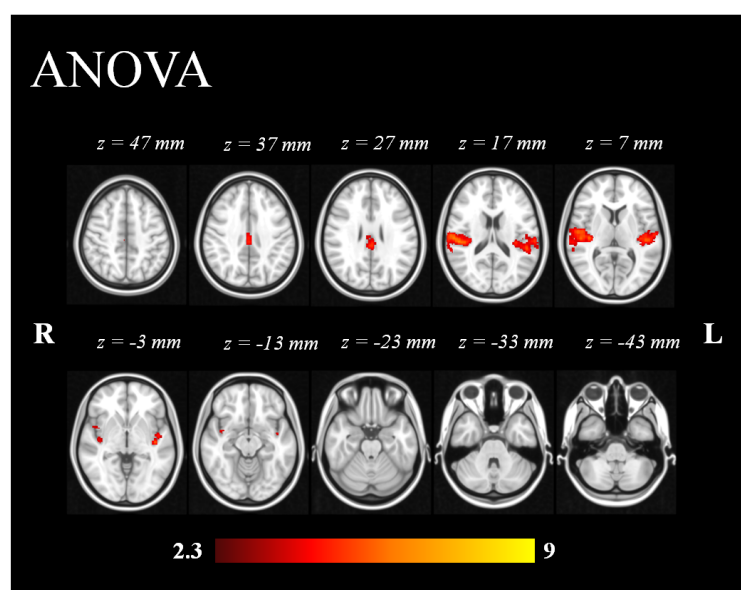


*Fig. 14: Repeated measures ANOVA of 1 factor at 4 levels.*

*Source: Own creation*

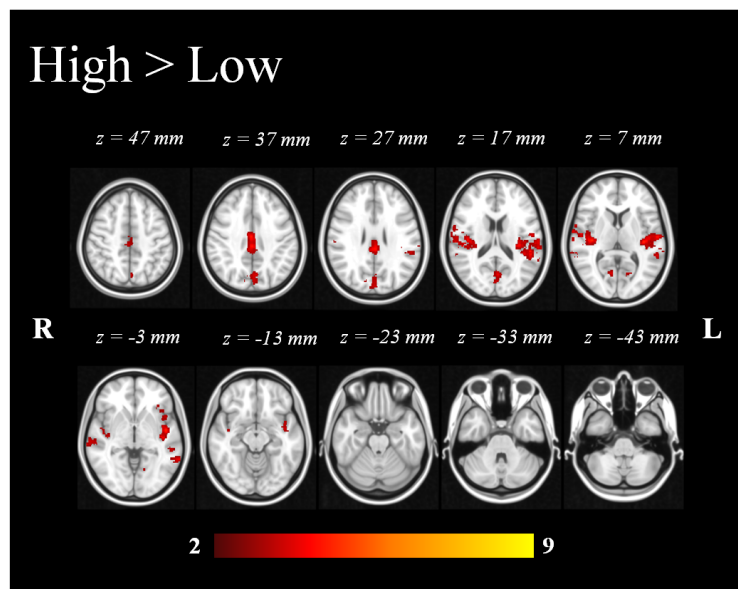


*Fig. 15: Fixed effects statistical map of EEG-informed group analysis ( $n = 16$ ) showing additional clusters in high vs. low intensity tones. Statistically significant voxels were thresholded at  $p < 0.05$ .*

*Source: Own creation*



## 8 Tables

	N	Mean	SD	Min.	Max.
Latency N1-peak 70 dB stimuli (ms)	16	170.00	18.53	136.00	204.00
Latency N1-peak 80 dB stimuli (ms)	16	157.50	11.85	132.00	176.00
Latency N1-peak 90 dB stimuli (ms)	16	149.75	8.13	136.00	164.00
Latency N1-peak 100 dB stimuli (ms)	16	150.25	5.46	140.00	156.00
Amplitude N1-peak 70 dB stimuli ( $\mu$ V)	16	-1.23	0.78	-2.44	0.57
Amplitude N1-peak 80 dB stimuli ( $\mu$ V)	16	-2.38	1.56	-4.80	-0.01
Amplitude N1-peak 90 dB stimuli ( $\mu$ V)	16	-3.26	1.72	-6.69	-0.96
Amplitude N1-peak 100 dB stimuli ( $\mu$ V)	16	-5.40	2.59	-8.90	-0.90
Latency P2-peak 70 dB stimuli (ms)	16	253.00	28.11	192.00	288.00
Latency P2-peak 80 dB stimuli (ms)	16	251.00	20.26	200.00	276.00
Latency P2-peak 90 dB stimuli (ms)	16	250.50	20.96	220.00	292.00
Latency P2-peak 100 dB stimuli (ms)	16	253.75	23.60	212.00	296.00
Amplitude P2-peak 70 dB stimuli ( $\mu$ V)	16	0.93	1.35	-0.71	4.35
Amplitude P2-peak 80 dB stimuli ( $\mu$ V)	16	2.14	1.62	0.16	6.72
Amplitude P2-peak 90 dB stimuli ( $\mu$ V)	16	3.61	2.32	-0.34	8.96
Amplitude P2-peak 100 dB stimuli ( $\mu$ V)	16	5.86	2.68	1.42	11.70

Tab. 1: Descriptive statistics of N1 and P2 ERPs.

Number of voxels	Max. Z	MNI coordinates of max.			Structures of max. (Harvard-Oxford Cortical and Subcortical Structural Atlases)
		X	Y	Z	
2885	7.2	54	-16	10	Right Planum Temporale, Right Heschl's Gyrus (includes H1 and H2), Right Central Opercular Cortex, Right Parietal Operculum Cortex, Right Superior Temporal Gyrus, posterior division
2269	5.74	-52	-24	8	Left Parietal Operculum Cortex, Left Heschl's Gyrus (includes H1 and H2), Left Planum Temporale, Left Central Opercular Cortex

*Tab. 2: Clusters of maximum with the 70 dB tones in the fMRI data analysis. Structures defined according to the Harvard-Oxford Cortical and Subcortical Structural Atlases.*

Number of voxels	Max. Z	MNI coordinates of max.			Structures of max. (Harvard-Oxford Cortical and Subcortical Structural Atlases)
		X	Y	Z	
3966	8.26	54	-16	10	Right Planum Temporale, Right Heschl's Gyrus (includes H1 and H2), Right Central Opercular Cortex, Right Parietal Operculum Cortex
2654	6.43	-52	-20	8	Left Parietal Operculum Cortex, Left Planum Temporale, Left Heschl's Gyrus (includes H1 and H2), Left Central Opercular Cortex

*Tab. 3: Clusters of maximum with the 80 dB tones in the fMRI data analysis. Structures defined according to the Harvard-Oxford Cortical and Subcortical Structural Atlases.*

Number of voxels	Max. Z	MNI coordinates of max.			Structures of max. (Harvard-Oxford Cortical and Subcortical Structural Atlases)
		X	Y	Z	
7638	9.88	54	-16	10	Right Heschl's Gyrus (includes H1 and H2), Right Central Opercular Cortex, Right Planum Temporale, Right Planum Polare, Right Parietal Operculum Cortex
6127	7.82	-52	-20	8	Left Parietal Operculum Cortex, Left Heschl's Gyrus (includes H1 and H2), Left Central Opercular Cortex, Left Planum Temporale

*Tab. 4: Clusters of maximum with the 90 dB tones in the fMRI data analysis. Structures defined according to the Harvard-Oxford Cortical and Subcortical Structural Atlases.*

Number of voxels	Max. Z	MNI coordinates of max.			Structures of max. (Harvard-Oxford Cortical and Subcortical Structural Atlases)
		X	Y	Z	
37867	12.1	56	-14	10	Right Central Opercular Cortex, Right Planum Temporale, Right Heschl's Gyrus (includes H1 and H2), Right Parietal Operculum Cortex, Right Planum Polare, Left Heschl's Gyrus (includes H1 and H2), Left Planum Temporale, Left Central Opercular Cortex, Left Planum Polare, Left Parietal Operculum Cortex

*Tab. 5: Clusters of maximum with the 100 dB tones in the fMRI data analysis. Structures defined according to the Harvard-Oxford Cortical and Subcortical Structural Atlases.*

Number of voxels	Max. Z	MNI coordinates of max.			Structures of max. (Harvard-Oxford Cortical and Subcortical Structural Atlases)
		X	Y	Z	
863	4.32	52	-14	6	Right Planum Polare, Right Heschl's Gyrus (includes H1 and H2), Right Insular Cortex
759	3.72	-48	-34	20	Left Heschl's Gyrus (includes H1 and H2), Left Parietal Operculum Cortex, Left Planum Temporale, Left Central Opercular Cortex

*Tab. 6: Clusters with maximal covariance with N1/P2 amplitudes at 70 dB in the fMRI data analysis. Structures defined according to the Harvard-Oxford Cortical and Subcortical Structural Atlases.*

Number of voxels	Max. Z	MNI coordinates of max.			Structures of max. (Harvard-Oxford Cortical and Subcortical Structural Atlases)
		X	Y	Z	
863	4.32	52	-14	6	Right Planum Polare, Right Heschl's Gyrus (includes H1 and H2), Right Insular Cortex
759	3.72	-48	-34	20	Left Heschl's Gyrus (includes H1 and H2), Left Parietal Operculum Cortex, Left Planum Temporale, Left Central Opercular Cortex

*Tab. 7: Clusters with maximal covariance with N1/P2 amplitudes at 80 dB in the fMRI data analysis. Structures defined according to the Harvard-Oxford Cortical and Subcortical Structural Atlases.*

Number of voxels	Max. Z	MNI coordinates of max.			Structures of max. (Harvard-Oxford Cortical and Subcortical Structural Atlases)
		X	Y	Z	
5567	5.15	62	-6	2	Right Insular Cortex, Right Planum Polare, Right Central Opercular Cortex
3996	4.39	-52	-18	6	Left Insular Cortex
2220	3.92	28	-62	28	Right Intracalcarine Cortex, Right Cuneal Cortex, Right Lingual Gyrus
1250	3.58	-6	0	54	Left Juxtapositional Lobule Cortex (formerly Supplementary Motor Cortex), Left Cingulate Gyrus, anterior division, Right Juxtapositional Lobule Cortex (formerly Supplementary Motor Cortex), Right Cingulate Gyrus, anterior division

*Tab. 8: Clusters with maximal covariance with N1/P2 amplitudes at 90 dB in the fMRI data analysis. Structures defined according to the Harvard-Oxford Cortical and Subcortical Structural Atlases.*



Number of voxels	Max. Z	MNI coordinates of max.			Structures of max. (Harvard-Oxford Cortical and Subcortical Structural Atlases)
		X	Y	Z	
1156	3.56	2	-86	8	Right Supracalcarine Cortex, Right Intracalcarine Cortex, Right Lingual Gyrus, Right Cuneal Cortex, Left Supracalcarine Cortex, Left Intracalcarine Cortex
790	3.64	40	0	-8	Right Frontal Operculum Cortex, Right Frontal Orbital Cortex, Right Inferior Frontal Gyrus, pars triangularis, Right Insular Cortex, Right Inferior Frontal Gyrus, pars opercularis
788	3.99	52	-44	58	Right Angular Gyrus, Right Supramarginal Gyrus, posterior division

*Tab. 9: Clusters with maximal covariance with N1/P2 amplitudes at 100 dB in the fMRI data analysis. Structures defined according to the Harvard-Oxford Cortical and Subcortical Structural Atlases.*

Area	Contrast							
	70 dB		80 dB		90 dB		100 dB	
	70 dB	N1/P 2	80 dB	N1/P 2	90 dB	N1/P 2	100 dB	N1/P 2
Accumbens						R + L	L	
Amygdala			R	R	R + L	R + L	R + L	
Angular Gyrus	R + L		R + L	L	R + L	R	R + L	R
Caudate				L	R + L	R + L	R + L	
Central Opercular Cortex	R + L	R	R + L	R + L	R + L	R + L	R + L	R
Cingulate Gyrus, anterior division					R	R + L	R + L	
Cingulate Gyrus, posterior division					R + L	R + L	R + L	R
Cuneal Cortex						R + L	R + L	R + L
Frontal Medial Cortex							R + L	
Frontal Operculum Cortex	R + L	R	R + L	R	R + L	R + L	R + L	R
Frontal Orbital Cortex		R	R	R	R + L	R + L	R + L	R
Frontal Pole					R + L	R + L	R	R
Heschl's Gyrus (includes H1 and H2)	R + L	R	R + L	R + L	R + L	R + L	R + L	R
Hippocampus					R + L	R + L	R + L	
Inferior Frontal Gyrus, pars opercularis	R + L	R	R	R	R + L	R + L	R + L	R
Inferior Frontal Gyrus, pars triangularis				R	R + L	R + L	R + L	R
Inferior Temporal Gyrus, anterior division						R		
Inferior Temporal Gyrus, posterior division						R	R	
Inferior Temporal Gyrus, temporooccipital part						R	R	
Insular Cortex	R + L	R	R + L	R + L	R + L	R + L	R + L	R
Intracalcarine Cortex						R + L	R + L	R + L
Juxtapositional Lobule Cortex						R + L	R + L	
Lateral Occipital Cortex, inferior division					R + L	R	R + L	L
Lateral Occipital Cortex, superior division					R + L	R + L	R + L	R + L
Lingual Gyrus					R + L	R + L	R + L	R + L
Middle Frontal Gyrus					R + L	R + L	R + L	
Middle Temporal Gyrus, anterior division	R + L	R	L	R	R + L	R	R + L	
Middle Temporal Gyrus, posterior division	R + L	R	R + L	R	R + L	R + L	R + L	
Middle Temporal Gyrus, temporooccipital part	R + L		R + L		R + L	R	R + L	
Occipital Fusiform Gyrus						R + L	R + L	R + L
Occipital Pole						R + L	R + L	R + L
Pallidum		R	R	L	R + L	R + L	R + L	
Paracingulate Gyrus						R + L	R + L	
Parahippocampal Gyrus, anterior division				R	R	R + L	R + L	
Parahippocampal Gyrus, posterior division					R + L		R + L	
Parietal Operculum Cortex	R + L	R	R + L	R + L	R + L	R + L	R + L	R
Planum Polare	R + L	R	R + L	R + L	R + L	R + L	R + L	R
Planum Temporale	R + L	R	R + L	R + L	R + L	R + L	R + L	R
Postcentral Gyrus	R + L	R	R + L	R + L	R + L	R + L	R + L	R
Precentral Gyrus	R + L	R	R + L	R	R + L	R + L	R + L	R
Precuneous Cortex						R + L	R + L	R + L
Putamen	R + L	R	R + L	R + L	R + L	R + L	R + L	R
Superior Frontal Gyrus						R + L	R + L	
Superior Parietal Lobule			L	L	R + L	R	R + L	R
Superior Temporal Gyrus, anterior division	R + L	R	R + L	R + L	R + L	R + L	R + L	
Superior Temporal Gyrus, posterior division	R + L	R	R + L	R + L	R + L	R + L	R + L	R
Supracalcarine Cortex						R + L	R + L	R + L
Supramarginal Gyrus, anterior division	R + L		R + L	L	R + L	R + L	R + L	R
Supramarginal Gyrus, posterior division	R + L		R + L	L	R + L	R + L	R + L	R
Temporal Fusiform Cortex, anterior division						R + L		
Temporal Fusiform Cortex, posterior division						R	L	
Temporal Occipital Fusiform Cortex							R + L	
Temporal Pole	R + L	R	R + L	R	R + L	R + L	R + L	R
Thalamus			R	L	R + L	R + L	R + L	

**Tab. 10: Complete list of the structures which exhibited activation with the four sound pressure levels in both analyses**

		70 dB	80 dB	90 dB	100dB
<b>Heschl's gyri</b>	fMRI	2554	3057	3825	4106
	EEG-informed fMRI	2782	3176	3864	4114
<b>Insular Cortices</b>	fMRI	583	872	2431	4353
	EEG-informed fMRI	844	1153	3033	4531
<b>Frontal Operculum</b>	fMRI	35	10	908	2276
	EEG-informed fMRI	110	106	1403	2417
<b>OFC</b>	fMRI	0	4	598	1482
	EEG-informed fMRI	11	39	1034	1612
<b>MFC</b>	fMRI	0	0	0	26
	EEG-informed fMRI	0	0	0	12
<b>ACC</b>	fMRI	0	0	1	2913
	EEG-informed fMRI	0	1	855	2827

*Tab. 11: Number of activated voxels ( $Z > 2.3$ ) in the selected ROIs*

*Source: Own creation*

Number of voxels	Max. Z	MNI coordinates of max.			Structures of max. (Harvard-Oxford Cortical and Subcortical Structural Atlases)
		X	Y	Z	
1448	4.71	50	-22	10	Heschl's Gyrus (includes H1 and H2), Planum Temporale, Parietal Operculum Cortex, Central Opercular Cortex
1306	4.74	-40	-20	0	Heschl's Gyrus (includes H1 and H2), Planum Temporale, Parietal Operculum Cortex, Central Opercular Cortex
448	3.89	0	-30	30	Cingulate Gyrus, posterior division, Cingulate Gyrus, anterior division

*Tab. 12: Cluster exhibiting significant intensity variation in the ANOVA*  
*. Structures defined according to the Harvard-Oxford Cortical and Subcortical Structural Atlases*

Number of voxels	Max. Z	MNI coordinates of max.			Structures of max. (Harvard-Oxford Cortical and Subcortical Structural Atlases)
		X	Y	Z	
2237	4.08	-40	-20	2	Left Heschl's Gyrus (includes H1 and H2), Left Planum Temporale, Left Superior Temporal Gyrus, posterior division
1252	4.44	56	-20	14	Right Heschl's Gyrus (includes H1 and H2), Right Planum Temporale, Right Central Opercular Cortex, Right Parietal Operculum Cortex
894	3.71	0	-28	38	Right Cingulate Gyrus, posterior division, Left Cingulate Gyrus, posterior division, Right Cingulate Gyrus, anterior division
738	3.02	-2	-70	18	Left Cuneal Cortex, Left Supracalcarine Cortex, Right Cuneal Cortex, Left Precuneous Cortex, Right Supracalcarine Cortex, Right Precuneous Cortex

*Tab. 13: Clusters exhibiting significant statistical difference in High > Low. Structures defined according to the Harvard-Oxford Cortical and Subcortical Structural Atlases*

## **9 Bibliography**

Allen, P.J., Josephs, O., Turner, R., 2000. A method for removing imaging artifact from continuous EEG recorded during functional MRI. *NeuroImage* 12, 230–9.

Allen, P.J., Polizzi, G., Krakow, K., Fish, D.R., Lemieux, L., 1998. Identification of EEG events in the MR scanner: the problem of pulse artifact and a method for its subtraction. *NeuroImage* 8, 229–39.

Angrilli, A., Bianchin, M., Radaelli, S., Bertagnoni, G., Pertile, M., 2008. Reduced startle reflex and aversive noise perception in patients with orbitofrontal cortex lesions. *Neuropsychologia* 46, 1179–84.

Augustine, J.R., 1996. Circuitry and functional aspects of the insular lobe in primates including humans. *Brain Research Reviews* 22, 229–44.

Bagshaw, A.P., Warbrick, T., 2007. Single trial variability of EEG and fMRI responses to visual stimuli. *NeuroImage* 38, 280–92.

Bamiou, D.-E., Musiek, F.E., Luxon, L.M., 2003. The insula (Island of Reil) and its role in auditory processing. Literature review. *Brain Research Reviews* 42, 143–54.

Beckmann, C.F., Jenkinson, M., Smith, S.M., 2003. General multilevel linear modeling for group analysis in FMRI. *Neuroimage* 20, 1052–63.

Blinowska, K., Müller-Putz, G., Kaiser, V., Astolfi, L., Vanderperren, K., Van Huffel, S., Lemieux, L., 2009. Multimodal imaging of human brain activity: rational, biophysical aspects and modes of integration. *Computational Intelligence and Neuroscience* 813607.

Brocke, B., Beauducel, A., John, R., Debener, S., Heilemann, H., 2000. Sensation seeking and affective disorders: characteristics in the intensity dependence of acoustic evoked potentials. *Neuropsychobiology* 41, 24–30.

Bushara, K.O., Grafman, J., Hallett, M., 2001. Neural correlates of auditory-visual stimulus onset asynchrony detection. *Journal of Neuroscience* 21, 300–4.

Calvert, G.A., Hansen, P.C., Iversen, S.D., Brammer, M.J., 2001. Detection of audio-visual integration sites in humans by application of electrophysiological criteria to the BOLD effect. *NeuroImage* 14, 427–38.

Da Costa, S., Van Der Zwaag, W., Marques, J.P., Frackowiak, R.S.J., Clarke, S., Saenz, M., 2011. Human Primary Auditory Cortex Follows the Shape of Heschl's Gyrus. *Journal of*

Neuroscience 31, 14067–14075.

Debener, S., De Vos, M., 2011. The benefits of simultaneous EEG-fMRI for EEG analysis. *Clinical Neurophysiology* 122, 217–8.

Debener, S., Herrmann, C.S., 2008. Integration of EEG and fMRI. Editorial. *International Journal of Psychophysiology* 67, 159–60.

Debener, S., Mullinger, K.J., Niazy, R.K., Bowtell, R.W., 2008. Properties of the ballistocardiogram artefact as revealed by EEG recordings at 1.5, 3 and 7 T static magnetic field strength. *International Journal of Psychophysiology* 67, 189–99.

Debener, S., Ullsperger, M., Siegel, M., Engel, A.K., 2006. Single-trial EEG-fMRI reveals the dynamics of cognitive function. *Trends in Cognitive Sciences* 10, 558–63.

Debener, S., Ullsperger, M., Siegel, M., Fiehler, K., von Cramon, D.Y., Engel, A.K., 2005. Trial-by-trial coupling of concurrent electroencephalogram and functional magnetic resonance imaging identifies the dynamics of performance monitoring. *The Journal of Neuroscience* 25, 11730–7.

Dierks, T., Barta, S., Demisch, L., Schmeck, K., Englert, E., Kewitz, A., Maurer, K., Poustka, F., 1999. Intensity dependence of auditory evoked potentials (AEPs) as biological marker for cerebral serotonin levels: effects of tryptophan depletion in healthy subjects.



Psychopharmacology 146, 101–7.

Downar, J., Crawley, A.P., Mikulis, D.J., Davis, K.D., 2000. A multimodal cortical network for the detection of changes in the sensory environment. *Nature Neuroscience* 3, 277–83.

Eichele, T., Specht, K., Moosmann, M., Jongsma, M.L.A., Quiroga, R.Q., Nordby, H., Hugdahl, K., 2005. Assessing the spatiotemporal evolution of neuronal activation with single-trial event-related potentials and functional MRI. *Proceedings of the National Academy of Sciences of the United States of America* 102, 17798–803.

Engelien, A., Silbersweig, D., Stern, E., Huber, W., Döring, W., Frith, C., Frackowiak, R.S., 1995. The functional anatomy of recovery from auditory agnosia. *Brain* 118, 1395–409.

Fox, P.T., Raichle, M.E., 1986. Focal physiological uncoupling of cerebral blood flow and oxidative metabolism during somatosensory stimulation in human subjects. *Proceedings of the National Academy of Sciences of the United States of America* 83, 1140–4.

Gallinat, J., Hegerl, U., 1994. Dipole source analysis. Linking scalp potentials to their generating neuronal structures. *Pharmacopsychiatry* 27, 52–3.

Heeger, D.J., Ress, D., 2002. What does fMRI tell us about

neuronal activity? *Nature Reviews Neuroscience* 3, 142–151.

Hegerl, U., Gallinat, J., Juckel, G., 2001. Event-related potentials. Do they reflect central serotonergic neurotransmission and do they predict clinical response to serotonin agonists? *Journal of Affective Disorders* 62, 93–100.

Hegerl, U., Gallinat, J., Mrowinski, D., 1994. Intensity dependence of auditory evoked dipole source activity. *International Journal of Psychophysiology* 17, 1–13.

Hegerl, U., Juckel, G., 1993. Intensity dependence of auditory evoked potentials as an indicator of central serotonergic neurotransmission: a new hypothesis. *Biological Psychiatry* 33, 173–87.

Hegerl, U., Juckel, G., 1994. Auditory evoked dipole source activity: indicator of central serotonergic dysfunction in psychiatric patients? *Pharmacopsychiatry* 27, 75–8.

Hegerl, U., Juckel, G., 2000. Identifying psychiatric patients with serotonergic dysfunctions by event-related potentials. *The World Journal of Biological Psychiatry* 1, 112–8.

Hegerl, U., Wulff, H., Müller-Oerlinghausen, B., 1992. Intensity dependence of auditory evoked potentials and clinical response to prophylactic lithium medication: a replication study. *Psychiatry*

Research 44, 181–90.

Hensch, T., Herold, U., Diers, K., Armbruster, D., Brocke, B., 2008. Reliability of intensity dependence of auditory-evoked potentials. *Clinical Neurophysiology* 119, 224–36.

Jenkinson, M., Bannister, P., Brady, M., Smith, S., 2002. Improved optimization for the robust and accurate linear registration and motion correction of brain images. *NeuroImage* 17, 825–41.

Juckel, G., Csépe, V., Molnár, M., Hegerl, U., Karmos, G., 1996. Intensity dependence of auditory evoked potentials in behaving cats. *Electroencephalography and Clinical Neurophysiology* 100, 527–37.

Juckel, G., Karch, S., Kawohl, W., Kirsch, V., Jäger, L., Leicht, G., Lutz, J., Stammel, A., Pogarell, O., Ertl, M., Reiser, M., Hegerl, U., Möller, H.J., Mulert, C., 2012. Age effects on the P300 potential and the corresponding fMRI BOLD-signal. *NeuroImage* 60, 2027–34.

Jung, T.P., Makeig, S., Humphries, C., Lee, T.W., McKeown, M.J., Iragui, V., Sejnowski, T.J., 2000. Removing electroencephalographic artifacts by blind source separation. *Psychophysiology* 37, 163–78.

Kawohl, W., Hegerl, U., Müller-Oerlinghausen, B., Juckel, G., 2008. [Insights in the central serotonergic function in patients with

affective disorders]. *Neuropsychiatrie* 22, 23–7.

Kiehl, K.A., Laurens, K.R., Duty, T.L., Forster, B.B., Liddle, P.F., 2001. Neural sources involved in auditory target detection and novelty processing: an event-related fMRI study. *Psychophysiology* 38, 133–42.

Koike, T., Kan, S., Misaki, M., Miyauchi, S., 2011. Connectivity pattern changes in default-mode network with deep non-REM and REM sleep. *Neuroscience Research* 69, 322–30.

Lauritzen, M., Gold, L., 2003. Brain function and neurophysiological correlates of signals used in functional neuroimaging. *The Journal of Neuroscience* 23, 3972–80.

Lee, T.-W., Yu, Y.W.Y., Chen, T.-J., Tsai, S.-J., 2005. Loudness dependence of the auditory evoked potential and response to antidepressants in Chinese patients with major depression. *Journal of Psychiatry & Neuroscience* 30, 202–5.

Logothetis, N.K., 2012. Intracortical recordings and fMRI: an attempt to study operational modules and networks simultaneously. *NeuroImage* 62, 962–9.

Logothetis, N.K., Pauls, J., Augath, M., Trinath, T., Oeltermann, A., 2001. Neurophysiological investigation of the basis of the fMRI signal. *Nature* 412, 150–7.

Makeig, S., Debener, S., Onton, J., Delorme, A., 2004. Mining event-related brain dynamics. *Trends in Cognitive Sciences* 8, 204–10.

Makeig, S., Jung, T.P., Bell, A.J., Ghahremani, D., Sejnowski, T.J., 1997. Blind separation of auditory event-related brain responses into independent components. *Proceedings of the National Academy of Sciences of the United States of America* 94, 10979–84.

Malonek, D., Dirnagl, U., Lindauer, U., Yamada, K., Kanno, I., Grinvald, A., 1997. Vascular imprints of neuronal activity: relationships between the dynamics of cortical blood flow, oxygenation, and volume changes following sensory stimulation. *Proceedings of the National Academy of Sciences of the United States of America* 94, 14826–31.

Malonek, D., Grinvald, A., 1996. Interactions between electrical activity and cortical microcirculation revealed by imaging spectroscopy: implications for functional brain mapping. *Science* 272, 551–4.

Mayhew, S.D., Dirckx, S.G., Niazy, R.K., Iannetti, G.D., Wise, R.G., 2010. EEG signatures of auditory activity correlate with simultaneously recorded fMRI responses in humans. *NeuroImage* 49, 849–64.

Mitzdorf, U., 1994. Properties of cortical generators of event-related potentials. *Pharmacopsychiatry* 27, 49–51.

Mulert, C., Jäger, L., Propp, S., Karch, S., Störmann, S., Pogarell, O., Möller, H.-J., Juckel, G., Hegerl, U., 2005. Sound level dependence of the primary auditory cortex: Simultaneous measurement with 61-channel EEG and fMRI. *NeuroImage* 28, 49–58.

Musall, S., von Pförtl, V., Rauch, A., Logothetis, N.K., Whittingstall, K., 2012. Effects of Neural Synchrony on Surface EEG. *Cerebral Cortex* 24, 1045–53

Niazy, R.K., Beckmann, C.F., Iannetti, G.D., Brady, J.M., Smith, S.M., 2005. Removal of FMRI environment artifacts from EEG data using optimal basis sets. *NeuroImage* 28, 720–37.

Norra, C., Becker, S., Bröcheler, A., Kawohl, W., Kunert, H.J., Buchner, H., 2008. Loudness dependence of evoked dipole source activity during acute serotonin challenge in females. *Human Psychopharmacology* 23, 31–42.

O'Neill, B. V, Croft, R.J., Nathan, P.J., 2008a. The loudness dependence of the auditory evoked potential (LDAEP) as an in vivo biomarker of central serotonergic function in humans: rationale, evaluation and review of findings. *Human Psychopharmacology* 23, 355–70.

O'Neill, B. V, Guille, V., Croft, R.J., Leung, S., Scholes, K.E., Phan, K.L., Nathan, P.J., 2008b. Effects of selective and combined

serotonin and dopamine depletion on the loudness dependence of the auditory evoked potential (LDAEP) in humans. *Human Psychopharmacology* 23, 301–12.

Ogawa, S., Lee, T.M., Kay, A.R., Tank, D.W., 1990. Brain magnetic resonance imaging with contrast dependent on blood oxygenation. *Proceedings of the National Academy of Sciences of the United States of America* 87, 9868–72.

Oostenveld, R., Praamstra, P., 2001. The five percent electrode system for high-resolution EEG and ERP measurements. *Clinical Neurophysiology* 112, 713–9.

Ostwald, D., Porcaro, C., Bagshaw, A.P., 2010. An information theoretic approach to EEG-fMRI integration of visually evoked responses. *NeuroImage* 49, 498–516.

Pissiota, A., Frans, O., Michelgård, A., Appel, L., Långström, B., Flaten, M.A., Fredrikson, M., 2003. Amygdala and anterior cingulate cortex activation during affective startle modulation: a PET study of fear. *The European Journal of Neuroscience* 18, 1325–31.

Rapin, I., Schimmel, H., Tourk, L.M., Krasnegor, N.A., Pollak, C., 1966. Evoked responses to clicks and tones of varying intensity in waking adults. *Electroencephalography and Clinical Neurophysiology* 21, 335–44.

Scherg, M., Vajsar, J., Picton, T.W., 1989. A source analysis of the late human auditory evoked potentials. *Journal of Cognitive Neuroscience* 1, 336–55.

Scherg, M., Von Cramon, D., 1986. Evoked dipole source potentials of the human auditory cortex. *Electroencephalography and Clinical Neurophysiology* 65, 344–60.

Smith, S.M., 2002. Fast robust automated brain extraction. *Human Brain Mapping* 17, 143–55.

Stuss, D.T., Benson, D.F., 1984. Neuropsychological studies of the frontal lobes. *Psychological Bulletin* 95, 3–28.

Woolrich, M., 2008. Robust group analysis using outlier inference. *Neuroimage* 41, 286–301.

Woolrich, M.W., Behrens, T.E.J., Beckmann, C.F., Jenkinson, M., Smith, S.M., 2004. Multilevel linear modelling for FMRI group analysis using Bayesian inference. *Neuroimage* 21, 1732–47.



## 10 Appendices

### Appendix I: Motion parameters of the single-level analyses

Subject	Absolute mean displacement (mm)	Relative mean displacement (mm)
1	1.06	0.09
2	0.46	0.06
3	2.03	0.13
4	1.17	0.22
5	1.19	0.12
6	0.86	0.08
7	0.75	0.34
8	1.15	0.07
9	0.72	0.08
10	0.74	0.05
11	0.52	0.05
12	1.04	0.11
13	0.66	0.21
14	1.12	0.1
15	2.72	0.16
16	0.97	0.08

Erklärung § 5 Abs. 1 zur Datenaufbewahrung

Hiermit erkläre ich, dass die dieser Dissertation zu Grunde liegenden Originaldaten bei meinem Betreuer,

***Univ.-Prof. Dr. N. Jon Shah, Institut für Neurowissenschaften und Medizin – 4,  
Forschungszentrum Jülich***

hinterlegt sind.



**Jorge Andrés Arrubla Martínez**



**Univ.-Prof. Dr. N. Jon Shah**

**Eidesstattliche Erklärung gemäß § 5 Abs. (1) und § 11 Abs. (3) 12. der Promotionsordnung**

Hiermit erkläre ich, **Herr Jorge Andrés Arrubla Martínez** an Eides statt, dass ich folgende in der von mir selbstständig erstellten Dissertation „Combined EEG and fMRI for the investigation of loudness dependence of auditory evoked potentials (LDAEP)“ dargestellten Ergebnisse erhoben habe:

Durchführung sämtlicher dargestellter Experimente (40%), sowie deren statistische Auswertung (100%).

Bei der Durchführung der Arbeit hatte ich folgende Hilfestellungen, die in der Danksagung angegeben sind:

- A. PD Dr. med. Irene Neuner: Studiendesign (33%), Durchführung sämtlicher dargestellter Experimente (20%), Anleitung der Auswertung (40%) und Korrektur des Manuskriptes (30%).
- B. PD Dr. med. Wolfram Kawohl: Studiendesign (33%), Durchführung sämtlicher dargestellter Experimente (20%), Anleitung der Auswertung (40%) und Korrektur des Manuskriptes (30%).
- C. Dr. Tracy Warbrick: Anleitung der Auswertung (20%) und Korrektur des Manuskriptes (4%).
- D. Dr. med. Konrad Hitz: Durchführung sämtlicher dargestellter Experimente (10%) und Korrektur des Manuskriptes (3%).
- E. Christine Wyss: Durchführung sämtlicher dargestellter Experimente (10%) und Korrektur des Manuskriptes (3%).
- F. Dipl.-Ing. Frank Boers: Aufstellung der auditorischen Stimulierung (100%).
- G. **Doktorvater** Univ.-Prof. Dr. N. Jon Shah: Studiendesign (34%) und –überwachung (100%), Korrektur des Manuskriptes (30%).

**Jorge Andrés Arrubla Martínez**

Als Betreuer der obigen Dissertation bestätige ich die Angaben von Herrn Jorge Andrés Arrubla Martínez

**Univ.-Prof. Dr. N. Jon Shah**